Defence Research and Development Canada
Recherche et développement pour la défense Canada

CAN UNCLASSIFIED

DRDC | RDDC
technologysciencetechnologie

A normal mode reverberation and target echo model to interpret towed array data in the Target and Reverberation Experiments

Dale D. Ellis
Member, IEEE

Jie Yang, John Preston
Life Member, IEEE

Sean Pecknold
DRDC – Atlantic Research Centre

IEEE Journal of Oceanic Engineering

Volume number: 42
Issue number: 2
Pagination info: 344–361

Date of Publication from Ext Publisher: April 2017

Defence Research and Development Canada
External Literature (P)
DRDC-RDDC-2018-P019
February 2018

CAN UNCLASSIFIED

IMPORTANT INFORMATIVE STATEMENTS

This document was reviewed for Controlled Goods by Defence Research and Development Canada (DRDC) using the Schedule to the *Defence Production Act*.

Endorsement statement: This publication has been peer-reviewed and published by the Editorial Office of Defence Research and Development Canada, an agency of the Department of National Defence of Canada. Inquiries can be sent to: Publications.DRDC-RDDC@drdc-rddc.gc.ca.

A Normal Mode Reverberation and Target Echo Model to Interpret Towed Array Data in the Target and Reverberation Experiments

Dale D. Ellis, *Member, IEEE*, Jie Yang, John R. Preston, *Life Member, IEEE*, and Sean Pecknold

***Abstract*—Reverberation measurements obtained with towed arrays are a valuable tool to extract information about the ocean environment. By superimposing a polar plot of reverberation beam time series on bathymetry maps, bottom features (often uncharted) can be located. As part of Rapid Environmental Assessment exercises, Preston and Ellis used directional reverberation measurements to extract environmental information using model-data comparisons. This early work used range-independent (flat bottom) ray-based models for the model-data comparisons, while current work includes range-dependent models based on adiabatic normal modes. Here, we discuss a range-dependent shallow-water reverberation model using adiabatic normal modes that has been developed to handle bottom scattering and clutter echoes in a range-dependent environment. Beam time series similar to those measured on a horizontal line array can be produced. Comparisons can then directly be made with data, features identified, and estimates of the scattering obtained. Of particular interest will be data obtained on the triplet line array during the 2013 Target and Reverberation EXperiments in the Gulf of Mexico off Panama City, FL, USA, where interesting effects in sea bottom sand dunes were observed. Particular attention has been paid to calibration to get estimates of scattering strengths. In addition to the reverberation, a preliminary investigation of the target echo is presented.**

***Index Terms*—Array signal processing, midfrequency reverberation, reverberation modeling, target echo.**

I. Introduction

REVERBERATION measurements obtained with towed arrays are a valuable tool to extract information about the ocean environment. Preston [1] pioneered the use of polar plots to display reverberation and identify scattering features. In that procedure, the towed array reverberation beam time series are mapped into range, beam angles into azimuth, and the resultant polar plot of reverberation intensity is superimposed on a bathymetry map around the source and receiver locations. Local peaks in reverberation generally coincide with bathymetric features; anomalous peaks in reverberation often coincide with uncharted bathymetric features. As part of Rapid Environmental Assessment exercises, Preston and Ellis [2], [3] used directional reverberation measurements to detect uncharted bottom features, and to extract environmental information using model-data comparisons.

This early work used range-independent (flat bottom) ray-based models for the model-data comparisons; current work includes range-dependent models based on adiabatic normal modes. This paper describes a range-dependent shallow-water model using adiabatic normal modes that has been developed to handle boundary scattering and target echoes in a range-dependent environment. Beam time series similar to that from a horizontal line array can be produced. Comparisons can then directly be made with data, and estimates of the scattering obtained.

Of particular interest are data obtained on the Five Octave Research Array (FORA) line array [4] during the Target and Reverberation EXperiments (TREX) in the Gulf of Mexico off Panama City, FL, USA in 2012 and 2013. The experiments were sponsored by the U.S. Office of Naval Research (ONR) and organized by the Applied Physics Laboratory at the University of Washington (APL/UW, Seattle, WA, USA). Their unique feature was a fixed source and fixed line array receiver deployed in about 20 m of water, over a period of several weeks. The acoustic experiments were complemented by an extensive set of environmental measurements to facilitate the understanding of the underlying reverberation and clutter mechanisms, and to support quantitative modeling. An overview of the experiment is summarized by Tang and Hefner [5], [6]. Preston [7] has presented an overview of some of the data, and an extensive analysis is presented in [8]. The initial model-data comparisons [9] suggested a correlation of the measured reverberation with the sand dunes, which was then confirmed [10] in the main set of experiments, though stronger than the model predicted.

The paper begins with a description of the normal-mode reverberation and target echo models, for monostatic and bistatic geometries, and flat and range-dependent environments. Section II describes the measurements from the recent TREX experiment. The main focus is on reverberation, but an initial look at the target echo is also included. Considerable effort was made to obtain calibrated data, and an appendix on calibrations

Manuscript received June 15, 2016; revised December 12, 2016; accepted February 20, 2017. Date of publication March 28, 2017; date of current version April 12, 2017. This work was supported by the U.S. Office of Naval Research, Ocean Acoustics, Code 32.

Guest Editors: B. T. Hefner and D. Tang.

D. D. Ellis is with the Department of Physics, Mount Allison University, Sackville, NB E4L 1E6 Canada (e-mail: daledellis@gmail.com).

J. Yang is with the Applied Physics Laboratory, University of Washington, Seattle, WA 98105 USA (e-mail: jieyang@apl.washington.edu).

J. R. Preston is with the Applied Research Laboratory, Pennsylvania State University, State College, PA 16804 USA (e-mail: jrp7@arl.psu.edu).

S. Pecknold is with the Atlantic Research Center, Defence Research and Development Canada, Dartmouth, NS B2Y 3Z7 Canada (e-mail: sean.pecknold@drdc-rddc.gc.ca).

Digital Object Identifier 10.1109/JOE.2017.2674106

is included. Section IV shows some model calculations, and model-data differences to help interpret and quantify the data. The model predictions follow the trend of the data reasonably well. However, as discussed in Section V, there are some high scattering features the model does not predict. At the current stage, no attempt has been made to model this high scattering. It seems to be related to some other scattering mechanism, so far undetermined, and detailed bottom measurements are necessary. The model has done its job—it tells us what we know, and the model-data differences show us where further investigation is needed.

II. Reverberation and Target Echo Model

An intensity-based formulation is used for the reverberation and target echo models. The essential concept is given by

$$R(t) = I_0 \int\!\!\int_{A(t)} \sum_m \sum_n H_m(r_{\rm mn}) S_{\rm mn} H_n(r_{\rm mn}) dA_{\rm mn} \quad (1)$$

where $R(t)$ is reverberation as a function of time, I_0 is the source intensity, H_m is propagation on the outgoing path from source to scatterer at range $r_{\rm mn}$, H_n is propagation on the incoming path from scatterer to receiver, $S_{\rm mn}$ is scattering from path m into path n, and $dA_{\rm mn}$ is the area insonified by the pulse. There are many outgoing and incoming paths, each with different travel times and scattering angles, so calculating the reverberation at a given time involves many different angles (and ranges).

For our approach the essential feature is to use normal modes for propagation, and ray-mode analogies for scattering. We begin with the range-independent monostatic case, with omnidirectional source and receiver. This was first described by Bucker and Morris [11], and later extended by Ellis [12]. The reverberation intensity at time t for a short pulse of intensity I_0 for duration τ_0 can be written as

$$\begin{aligned} R_0(t) = \; & I_0 \tau_0 (2\pi)^3 \rho_w^{-4} \sum_{n=1}^{N} k_n^{-1} \left[u_n(z_S) A_n(z_b)\right]^2 \\ & \times \sum_{m=1}^{N} k_m^{-1} \left[u_m(z_R) A_m(z_b)\right]^2 C_{\rm nm} r_{\rm nm}^{-1} S_b(\theta_{\rm nb}, \theta_{\rm mb}) \\ & \times \exp[-2(\delta_n + \delta_m) r_{\rm nm}] \end{aligned} \quad (2)$$

where ρ_w is the density[1] in the water column, b refers to the boundary (surface or bottom), S_b is the scattering function at the boundary, z_b is the surface or bottom boundary depth, z_S and z_R are the source and receiver depths, u_n, A_n, k_n, δ_n, and g_n are the mode functions, amplitudes, wave numbers, attenuations, and group speeds, respectively. The θ_n are the equivalent ray grazing angles of the modes at the boundary depths, and $r_{\rm nm} = g_n t_n = g_m t_m$, where $t = t_n + t_m$, with t_n and t_m being the travel times from the source (or receiver) to the scattering patch. The summations are over the number of modes. Note $C_{\rm nm} = \omega/(k_n + k_m)$, where $\omega = 2\pi f$ is the angular frequency, is an area adjustment factor that basically reduces to half the average phase speed $c_p/2$.

The formulation can be extended to handle beam patterns, bistatic reverberation, and range dependence, as well as target echo. These are described in the following sections, along with two models based on these formulations.

A. Range-Independent Monostatic Reverberation With Beam Patterns

Following [12], but adding beam patterns [13], reverberation level at time t for a short pulse of intensity I_0 for duration τ_0 and a beam steered in the direction β_l can be written as

$$\begin{aligned} R_0(t, \beta_l) = \; & I_0 \tau_0 (2\pi)^3 \rho_w^{-4} \sum_{n=1}^{N} k_n^{-1} B_S(\theta_{\rm nS}) \left[u_n(z_S) A_n(z_b)\right]^2 \\ & \times \sum_{m=1}^{N} k_m^{-1} B_{Rl}(\theta_{\rm mR}) \left[u_m(z_R) A_m(z_b)\right]^2 C_{\rm nm} r_{\rm nm}^{-1} \\ & \times S_b(\theta_{\rm nb}, \theta_{\rm mb}) \exp[-2(\delta_n + \delta_m) r_{\rm nm}] \end{aligned} \quad (3)$$

where B_S is the source beam pattern, B_{Rl} is the (effective) beam pattern of the lth receiver beam and $\theta_{n[S,R,b]}$ are the equivalent ray grazing angles of the modes at the source, receiver, and boundary depths.

Implicit in (3) is an azimuthal angular independence. For directional receivers, such as towed arrays, one would have to compute the reverberation over azimuthal angles. However, the angular integration can be avoided by precomputing the effective receiver vertical beam pattern [14] or reverberation response over a flat uniform bottom, which is the towed array beam pattern $B_R(\theta, \phi; \beta_l)$ at vertical angle θ integrated over all azimuth angles ϕ

$$B_{\rm eff}(\theta; \beta_l) = \frac{1}{2\pi} \int_0^{2\pi} B_R(\theta, \phi; \beta_l)\, {\rm d}\phi. \quad (4)$$

where β_l is the steering angle of the towed array.

The average up- and down-going beam patterns are needed for the normal-mode formulation

$$B_{Rl}(\theta) = \left[B_{\rm eff}(-\theta; \beta_l) + B_{\rm eff}(\theta; \beta_l)\right]/2. \quad (5)$$

For towed array beams away from the endfire region, the vertical angle dependence of $B_{Rl}(\theta)$ at low grazing angles is fairly constant (see figures in [14]). Since the reverberation in the waveguide arrives also at low-grazing angles, the quantity $B_{Rl}(0)$ can be interpreted as an effective reverberation reduction, or equivalently as an equivalent horizontal beamwidth/(2π) that includes the effect of any sidelobes [15].

B. Bistatic Reverberation: Range Independent

The equation for bistatic reverberation looks essentially the same as the monostatic equation (3), except that: 1) the reverberation depends on azimuthal angle ϕ (measured counter clockwise from the receiver, with the source at $\phi = \pi$); 2) the scattering function $S_b(\theta_m, \theta_n, \psi)$ depends on the bistatic angle ψ between the source-scatterer-receiver (see Fig. 1); and 3) one must use the actual three-dimensional (3-D) beam patterns, not

[1]The density, needed for consistency with the normal mode normalization, was omitted from [12].

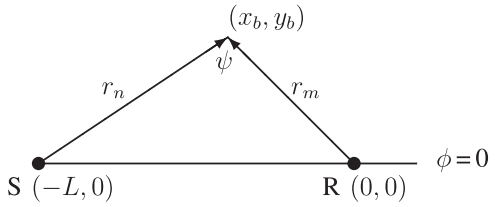

Fig. 1. Bistatic geometry, with $(0, 0)$, $(-L, 0)$, and (x_b, y_b) being the receiver R, source S, and scatterer locations in Cartesian coordinates.

the effective beam patterns. In terms of the mode functions, the equation can be written as

$$\begin{aligned} R_0(t,\beta_l) = \; & I_0 \tau_0 (2\pi)^2 \rho_w^{-4} \int_0^{2\pi} \mathrm{d}\phi \sum_{n=1}^{N} k_n^{-1} B_S(\theta_{nS}, \phi) \\ & \times \left[u_n(z_S) A_n(z_b)\right]^2 \sum_{m=1}^{N} k_m^{-1} B_R(\theta_{mR}, \phi; \beta_l) \\ & \times \left[u_m(z_R) A_m(z_b)\right]^2 S_b(\theta_{\mathrm{nb}}, \theta_{\mathrm{mb}}, \psi) \\ & \times \exp[-2(\delta_n r_{\mathrm{mn}} + \delta_m r_{\mathrm{mn}})] r_{\mathrm{mn}}^{-1} C'_{\mathrm{nm}}(\phi). \quad (6) \end{aligned}$$

The area adjustment factor $C'_{\mathrm{mn}}(\phi)$ is similar to the $\omega/(k_n + k_m)$ term in the monostatic case, but more complicated [13], [16].

C. Bistatic Reverberation: Range-Dependent Adiabatic Modes

The group velocity time dependence adds a lot of complexity to the formulation, so we drop it for the range-dependent formulation. It is an $N \times 2D$ formulation; i.e., there is no horizontal refraction. The propagation paths are over a range-dependent geometry, but with adiabatic modes the result looks very similar to (6); i.e.,

$$\begin{aligned} R_0(t,\beta_l) = \; & I_0 \tau_0 (2\pi)^2 \rho_w^{-4} \int_{\phi_{\mathrm{min}}}^{\phi_{\mathrm{max}}} \mathrm{d}\phi \sum_{n=1}^{N_{\mathrm{Sb}}} \overline{k}_{\mathrm{nSb}}^{-1} B_S(\theta_{\mathrm{nS}}, \phi) \\ & \times \left[u_n(z_S; x_S, y_S) A_n(z_b; x_b, y_b)\right]^2 \\ & \times \sum_{m=1}^{N_{\mathrm{Rb}}} \overline{k}_{\mathrm{mRb}}^{-1} B_R(\theta_{\mathrm{mR}}, \phi; \beta_l) \\ & \times \left[u_m(z_R; x_R, y_R) A_m(z_b; x_b, y_b)\right]^2 \\ & \times \frac{S_b(\theta'_{\mathrm{nb}}, \theta'_{\mathrm{mb}}, \psi; x_b, y_b)}{r_{\mathrm{Sb}}} \\ & \times \exp[-2(\overline{\delta}_{\mathrm{nSb}} r_{\mathrm{Sb}} + \overline{\delta}_{\mathrm{mRb}} r_{\mathrm{Rb}})] \\ & \times C'_{\mathrm{nm}}(\phi, r_{\mathrm{Sb}}, r_{\mathrm{Rb}}). \quad (7) \end{aligned}$$

The source is at x_S, y_S, the receiver is at x_R, y_R, and the bottom scattering takes place at x_b, y_b. The wave number and attenuation coefficients, $\overline{k}_{\mathrm{nSb}}, \overline{k}_{\mathrm{mRb}}, \overline{\delta}_{\mathrm{nSb}}, \overline{\delta}_{\mathrm{mRb}}$, are averaged over the source–scatterer path or scatterer–receiver path; e.g., $\overline{k}_{\mathrm{nSb}}(r) = r^{-1} \int_{[x_S, y_S]}^{[x_b, y_b]} k_n(r) dr$. The scattering angles at the bottom are modified by the local slope $\chi(r)$ along each radial; i.e., $\theta'_{\mathrm{nb}}(r) = \max(0, \theta_{\mathrm{nb}} + \chi(r))$. The summations are over the minimum number of modes along the source–scatterer path or scatterer–receiver path. Range is mapped into time with some average group velocity: $t = (r_{\mathrm{Sb}} + r_{\mathrm{Rb}})/c_g$; the area correction $C'_{\mathrm{mn}}(\phi)$ is now independent of m and n.

The azimuthal integration limits are $\phi_{\mathrm{min}} = 0$ and $\phi_{\mathrm{min}} = 2\pi$. In practice, we may want to integrate over only an azimuthal sector; e.g., where outside this region the beam pattern may be sufficiently small that the contributions are negligible.

D. Target Echo

The target echo in the monostatic range-independent case follows Ellis *et al.* [17]

$$\begin{aligned} T_e(t,\beta_l; r, \phi_T) = \; & (2\pi/r)^2 \rho_w^{-4} \sum_{n=1}^{N} k_n^{-1} B_S(\theta_{\mathrm{nS}}, \phi_T) \\ & \times \left[u_n(z_S) A_n(z_T)\right]^2 \\ & \times \sum_{m=1}^{N} k_m^{-1} B_R(\theta_{\mathrm{mR}}, \phi_T; \beta_l) \\ & \times \left[u_m(z_R) A_m(z_T)\right]^2 \\ & \times \exp[-2(\delta_n + \delta_m) r] E_{\mathrm{nm}}(z_T) \\ & \times I_0(t - t_n - t_m) \quad (8) \end{aligned}$$

where z_T is the target depth, E_{nm} is the target echo strength (which can be angle dependent), and $t_n = r/g_n$ are the mode travel times to the target. The mode amplitude envelopes A_n are used, which would be most appropriate for a target distributed over depth [17]. For a point target one would use the mode functions $u_n(z_T)$. Note in this case the receiver beam pattern B_R is a vertical section at azimuth ϕ_T, and *not* integrated over azimuth.

Extending (8) to range-dependent bistatic geometry using adiabatic modes gives

$$\begin{aligned} T_e(t,\beta_l; x_T, y_T) = \; & \frac{(2\pi)^2}{r_{ST} r_{\mathrm{RT}}} \rho_w^{-4} \sum_{n=1}^{N_{\mathrm{ST}}} \overline{k}_{\mathrm{nST}}^{-1} B_S(\theta_{\mathrm{nS}}, \phi_T) \\ & \times \left[u_n(z_S; x_S, y_S) A_n(z_T; x_T, y_T)\right]^2 \\ & \times \sum_{m=1}^{N_{\mathrm{RT}}} \overline{k}_{\mathrm{mRT}}^{-1} B_R(\theta_{\mathrm{mR}}, \phi_T; \beta_l) \\ & \times \left[u_m(z_R; z_R, y_R) A_m(z_T; x_T, y_T)\right]^2 \\ & \times \exp\left[-2(\overline{\delta}_{\mathrm{nST}} r_{\mathrm{ST}} + \overline{\delta}_{\mathrm{mRT}} r_{\mathrm{RT}})\right] \\ & \times E_{\mathrm{nm}}(z_T, \psi; x_T, y_T) I_0(t - t_n - t_m). \end{aligned} \quad (9)$$

As with the reverberation calculation, the wave numbers $\overline{k}_{\mathrm{nSt}}$ and attenuations $\overline{\delta}_{\mathrm{nSt}}$ are averaged over the source-target path or target-receiver path, and the summations are over the minimum number of modes along the corresponding path.

Note that in the case of constant group velocities, if E_{nm} is independent of m and n, there are no cross terms in (8) and (9), so the double summation reduces to the product of two single sums. Ignoring the time spreading for reverberation will

probably not produce serious errors, however, for a short pulse it may not be a good approximation in the target echo calculation.

E. Clutter Model

The Clutter Model [16], [18], [19] implements (7) and (9) over an area. The modes are calculated on a series of grid points, and the amplitudes along each radial (slowly varying compared to the mode functions themselves) obtained by 2-D linear interpolation. The internal computational subroutine can handle an arbitrary sound-speed profile and layered bottom at each grid point, and reflection losses from surface and bottom rms roughness can be included [20]. At present the calling program is not that general, so is mainly limited to changes in the bathymetry. In principle any separable scattering function can be used at either the surface, bottom or sub-bottom interface. In practice only Lambert bottom scattering has been implemented, though an arbitrary scattering strength can be specified at each grid point.

A key component is how the model handles the towed array beam patterns. The azimuthal integration is broken into a specified number of radials at azimuths $\phi_j, j = 1, \ldots, N_j$ measured from the receiver. Often the receiver beam pattern is quite narrow, but the environment may not be varying much. In this case, for computational efficiency, an effective beam pattern is precomputed over the sector j, where the integration of (4) is over the interval $[(\phi_{j-1} + \phi_j)/2, (\phi_j + \phi_{j+1})/2]$.

In the FORA array (see Section III-A) each element of the line array is composed of three elements (triplets), which can be used to form broadside cardioids steered left or right. The total array beam pattern B_T is then the usual line array beam pattern B_L multiplied by broadside cardioids B_C; i.e.,

$$B_T(\theta, \phi) = B_L(\beta; \beta_l) B_C(\beta; \beta_l) \tag{10}$$

where $\cos\beta = \cos\theta \cos\phi$, $B_C = [(1 \pm \sin\beta)/(1 + |\sin\beta_l|)]^2$, with β is measured from forward endfire, and the $\pm$ determines right or left broadside. The cardioid gives unit response at the linear array steering angle β_l, a null on the opposite broadside, and no singularity on the endfire beams.

In addition to the reverberation effects due to bottom bathymetry, the Clutter Model can handle a number of scattering objects of arbitrary strength, at arbitrary locations $(x_{\mathrm{Tc}}, y_{\mathrm{Tc}}, z_{\mathrm{Tc}})$. These are modeled as point targets, (9), hence the name Clutter Model. Each run is deterministic, and does not include any statistics.

Typically, the Clutter Model is used to model the full set of beams from a towed array, and display the results as a polar plot for the area. For realism and model-data comparisons it also has the option of specifying a constant noise level on each beam.

F. Separable Approximation; Monostatic Geometry; R2D3 Model

If the scattering function can be written in separable form; e.g., $S(\theta_m, \theta_n) = b(\theta_m) b(\theta_n)$, then for monostatic geometry the double sum of (7) can be written as a product of two single sums [12], [21]

$$R(t) = A_0 F_S(r) F_R(r) \tag{11}$$

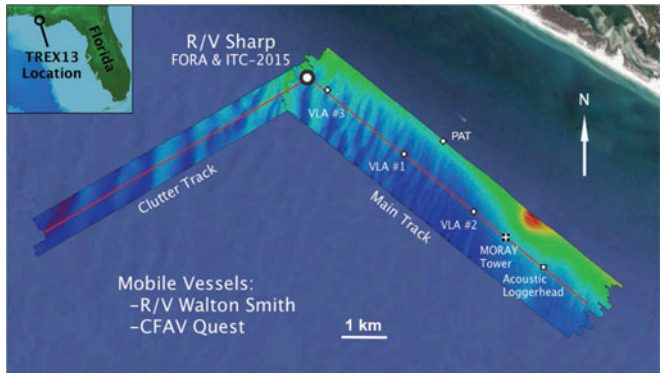

Fig. 2. TREX13 site showing bathymetry and deployments. The source and FORA horizontal array are fixed near bottom in about 20-m water. Water depths range from 12 (red) to 21 m (dark blue); the main track is about 7 km and of nearly constant depth sand dunes are 1–2 m in height, and several hundred meters apart.

where $A_0 = I_0 \tau_0 (2\pi)^2 r^{-1} \rho_w^{-4} \Phi$

$$F_S(r) = \sum_n B_S(\theta_{\mathrm{nS}}) u_n^2(z_S; 0) A_n^2(z_b; r) b(\theta'_{\mathrm{nb}}; r) \times \exp(-2\overline{\delta}_n r)(\overline{k}_n)^{-1} \tag{12}$$

and Φ is the effective horizontal beamwidth or some other angular sector of interest. F_R is given by a similar expression for the receiver.

Our calculations here have generally assumed Lambert's rule for bottom scattering; i.e., $S(\theta_m, \theta_n) = \mu \sin(\theta_m) \sin(\theta_n)$, where μ is the Lambert scattering strength, adjustable to fit the data, but typically 0.002, and usually quoted in decibel (here -27 dB).

The R2D3 model provides an implementation of (7) without beam patterns, and along a single radial. It can handle an arbitrary sound-speed profile and layered bottom at multiple range points. In principle any scattering function can be used at either the surface, bottom or sub-bottom interface; in practice only bottom scattering has been implemented, Lambert ($\sin^2$) or $\sin^4$. Losses from surface and bottom rms roughness can be included. Beam pattern effects are approximated by setting Φ to the effective horizontal beamwidth obtained from the effective reverberation response described at the end of Section II-A. R2D3 has the option that $b(\theta'_{\mathrm{nb}}; r)$ may include, or not include, the bottom slope.

It also calculates the target echo as a function of range, with (9) reduced to

$$T_e(r) = \frac{(2\pi)^2 E_T}{r^2 \rho^4} \sum_{n=1}^{N_r} \overline{k}_n^{-1} u_n^2(z_S; 0) A_n^2(z_T; r) e^{-2\overline{\delta}_n r} \times \sum_{m=1}^{N_r} \overline{k}_n^{-1} u_m^2(z_R; 0) A_m^2(z_T; r) e^{-2\overline{\delta}_m r} \tag{13}$$

where E_T is the target strength, and $r = c_g t/2$ with c_g being an average group velocity for all modes.

The R2D3 model is typically used to obtain line plots for comparison with a single beam of the towed array. Higher resolution bathymetry on a single radial can be incorporated.

TABLE I
BEST ESTIMATES OF SOURCE-RECEIVER GEOMETRY AND LOCATIONS

Date	ITC		Approx.	FORA			
Runs Julian day	location Lat (°N)	Lon (°W)	source-receiver geometry	Nominal heading	Estimated orientation	Module center Lat (°N)	Lon (°W)
Apr 23–26 Runs 11–32 JD113–116	30.05977	85.68056	source 3-m NW of FORA center	219	217	30.05976	85.68054
Apr 26-May 1 Runs 33–53 JD116–122	30.05968	85.68107	source 50-m W of FORA	219	217	30.05976	85.68054
May 7 Runs 58–62 JD127	30.05975	85.68084	source 62.5-m N of FORA center	333	334	30.05927	85.68058
May 8–17 Runs 63–131 JD128–136	30.05975	85.68084	source 62.5-m N of FORA center	358	356	30.05925	85.68063
2012 Apr 20 JD111	30.059868 (location of *R/V Sharp*)	85.681053	source about 5-m W of FORA	007		30.059492 (derived location)	85.681116

The first four entries are from TREX13, and the last entry is from the 2012 experiment. The heading/orientations in the table have been corrected for magnetic declination 3° W of N.

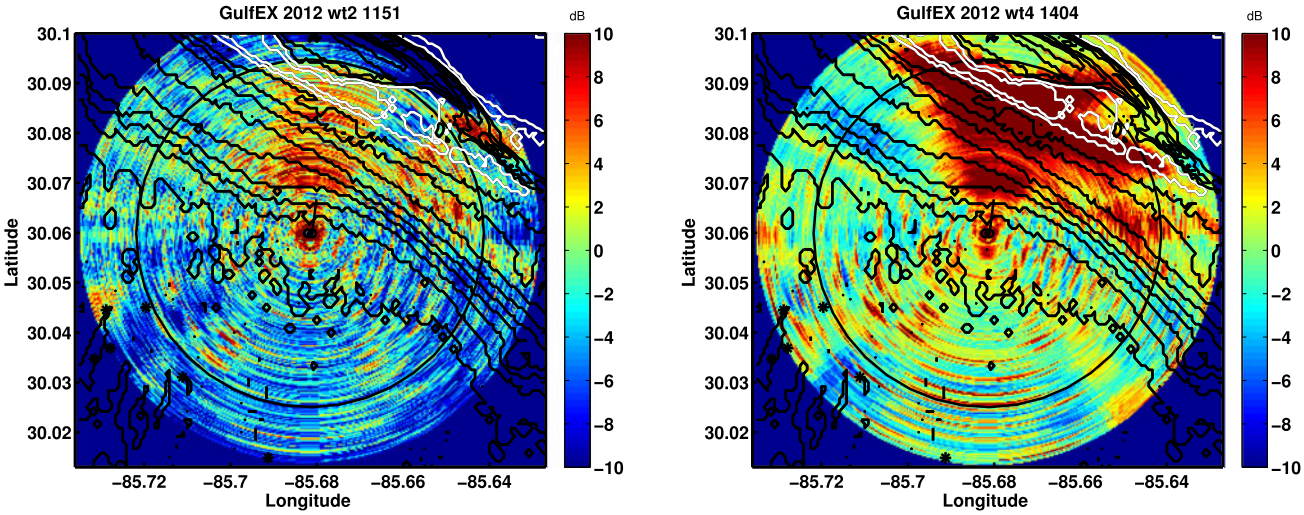

Fig. 3. Plots of model-data differences for a short CW pulse (left) and a LFM pulse (right) in 2012.

III. MEASUREMENTS OF REVERBERATION AND TARGET ECHO

As mentioned in Section I, TREX was a series of Target and Reverberation Experiments off Panama City, FL, USA. Their unique feature was a fixed source and fixed receiver deployed in about 20 m of water, with the acoustic experiments being complemented by an extensive set of environmental measurements to facilitate the understanding of the underlying reverberation and clutter mechanisms, and to support quantitative modeling. In this section, we look at some of the measurements of reverberation and target echo data received on a horizontal line array with triplet elements, which enable left–right discrimination.

A. TREX Reverberation Experiments

An initial work-up experiment was conducted in April 2012 with a fixed source (ITC-2015) and receiver (the triplet section of FORA [4]) deployed from *Research Vessel (R/V) Sharp*. The same equipment was deployed in the main TREX13 experiment conducted in April and May 2013. In addition, for part of the time in 2013, Defence Research and Development Canada (DRDC) participated with their *Canadian Forces Auxiliary Vessel (CFAV) Quest*, towing an echo repeater for transmission loss and target echo measurements, as well as conducting active sonar experiments [22]. Other equipments were deployed, including the Scripps vertical line arrays (VLAs) for transmission loss measurements, and a DRDC passive acoustic target (PAT), a vertical air-filled hose spanning most of the water column for echo measurements from a fixed location. Fig. 2 illustrates the TREX13 site, with the two arms representing fine scale bathymetry in the main reverberation and Clutter Tracks.

The source–receiver pair were deployed in fixed positions several times during the experiment (see Table I). Even though the array was stretched between fixed poles, the array compass varied a few degrees run-to-run and ping-to-ping, possibly due

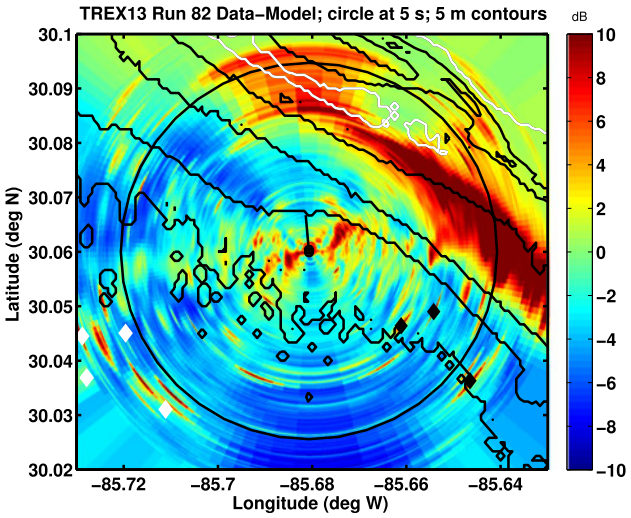

Fig. 4. TREX13 example: Model-data differences for 1800–2700-Hz LFM signal. Reverberation level is uncalibrated, with model level adjusted to agree near array. Large differences are observed near the shoreline (white contour). Many clutter objects stand out; some of these are correlated with known objects (filled diamonds).

to currents. The estimated orientation is obtained from the maximum beam response from location of known scattering objects; e.g., the VLA and PAT air hose. Locations for 2012 were taken from the log file for the JD111 1404Z pulse; the ITC location is actually the position of the GPS on *R/V Sharp*, and the FORA location is derived from the cable scope and presumed bearing.

During TREX13, reverberation data were taken during all hours of the day and night, allowing study of reverberation variation over time and sea surface conditions. In addition to the time and weather dependence, the full 360° directional dependence of reverberation level could be determined using the FORA triplet array. The focus of the experiment was on reverberation returning from a track of relatively uniform water depth of 20 m, extending about 10 km to the SE (129 °T) of the source and receiver. A secondary focus was the Clutter Track, extending to the SW (240 °T) toward some known bottom scattering objects.

The ITC-2015 source was deployed from *R/V Sharp*, 1.2 m above the bottom. A large variety of pulses were used in the experiments. Of particular interest here are various pulses between 1800 and 3600 Hz, with the latter frequency being near the design frequency of the FORA triplet array. Typical Applied Research Laboratory (ARL)/APL pulses were: 1-s CWs at 1900, 2700, and 3500 Hz; 1-s 100-Hz bandwidth LFMs centered at 1950, 2750, and 3450 Hz; wideband pulses of 1800–2700 Hz, 2700–3600 Hz, and 1800–3600 Hz. All pulses had $\sin^2$ tapering at each end (10% Tukey shading). Their input voltage to the signal generator was flat; so the output levels followed the frequency output of the source; e.g., 196.1, 197.8, and 196.4 dB (re 1 μPa^{2}m^2) at 1.9, 2.7, and 3.5 kHz, respectively.[2] Typical DRDC pulses were: 0.5-s CWs at 1900, 2700, and 3500 Hz; 0.5 s 200-Hz bandwidth LFMs centered at 1900, 2700, and 3500 Hz; several 0.5-s wideband LFMs: 1800–2700 Hz, 2700–3600 Hz, and 1800–3600 Hz. All had 5% Tukey tapering at each end. Their inputs to the signal generator were shaped to have a flat response of 198.5 dB re 1 μPa^{2}m^2 over the frequency band for each pulse. After May 7, the high band ($>$ 2700 Hz) DRDC LFM pulses were not used. The energy source levels (ESL) are the source intensity times the pulse length reduced by the Tukey shading (0.6 dB for 10% shading).

The receiver was the triplet section of FORA [4], an ONR array designed and maintained by the ARL at The Pennsylvania State University (PSU, State College, PA, USA). The triplet section of FORA has 78 elements at 0.2-m spacing, which implies a design frequency of 3750 Hz for a sound speed of 1500 m/s. Each element of the line array is composed of three elements (triplets), which can be used to form broadside cardioids steered left or right [23]. For the TREX experiments it was deployed horizontally in a fixed position, between two fixed vertical posts, 2.1 m above the bottom. For this experiment only the 48-element rear subsection of the triplet was used, with an array length about 9.4 m, or roughly 22 wavelengths at 3500 Hz (12 λ at 1900 Hz).

Though over-resolving, to maintain consistency with beam angles from other experiments, for the ARL and DRDC processing these 48 working elements were Hann-weighted and used to form 157 beams, 79 equally spaced in the sine of the beam steering angle, from forward to aft endfire on each side. The triplets in each element were used to form broadside cardioids on the appropriate side, except at aft endfire where only the right-looking cardioid was used. (Beam 1 is forward endfire, Beam 40 is right broadside, Beam 79 is endfire, and Beam 118 is left broadside.) The APL processing typically used uniform weighting of the elements, and formed beams at 1° bearing increments; details are in [8].

After beamforming, the beam time series were match filtered. The DRDC matched filter (MF) was not normalized. The ARL MF was normalized so that the reverberation was reduced by approximately the time-bandwidth product. The APL MF was normalized so that the reverberation levels approximated energy. A procedure was developed to resolve the various calibrations; see Appendix A.

B. Reverberation Data

1) GulfEx 2012 Data: In 2012, a small "pre-experiment" to test the systems and procedures had been conducted. FORA was deployed with the forward endfire beam pointing 7° E of N. The source was an ITC-2015 transducer, operating at 199 dB (re 1 μPa^{2}m^2). It had an omnidirectional beam pattern and was deployed 1.2 m off the bottom, about 3-mW of the midpoint of the FORA array. Generally, pulses were sent every 30 s; for each pulse, 25 s of data were recorded with 1 s of background noise before the pulse. The main pulses sent were 0.8-ms continuous wave (CW) at 3500 Hz, 10-ms CW at 3500 Hz, and 100-ms LFM from 2500–3500 Hz. The short 0.8-ms pulse was used as a calibration pulse, with the direct and bottom bounce arrivals separated in time. The other two signals were used to test the signal range; e.g., the 100-ms LFM could stay above background noise for $\sim$5 s.

[2]For narrowband pulses near 3.5 kHz, the amplifier voltage was often increased to produce a source level of 199.4 dB. After May 7, the L10 amplifier on the ITC-2015 source was replaced by an L6 amplifier, which reduced the maximum output levels by 1 dB.

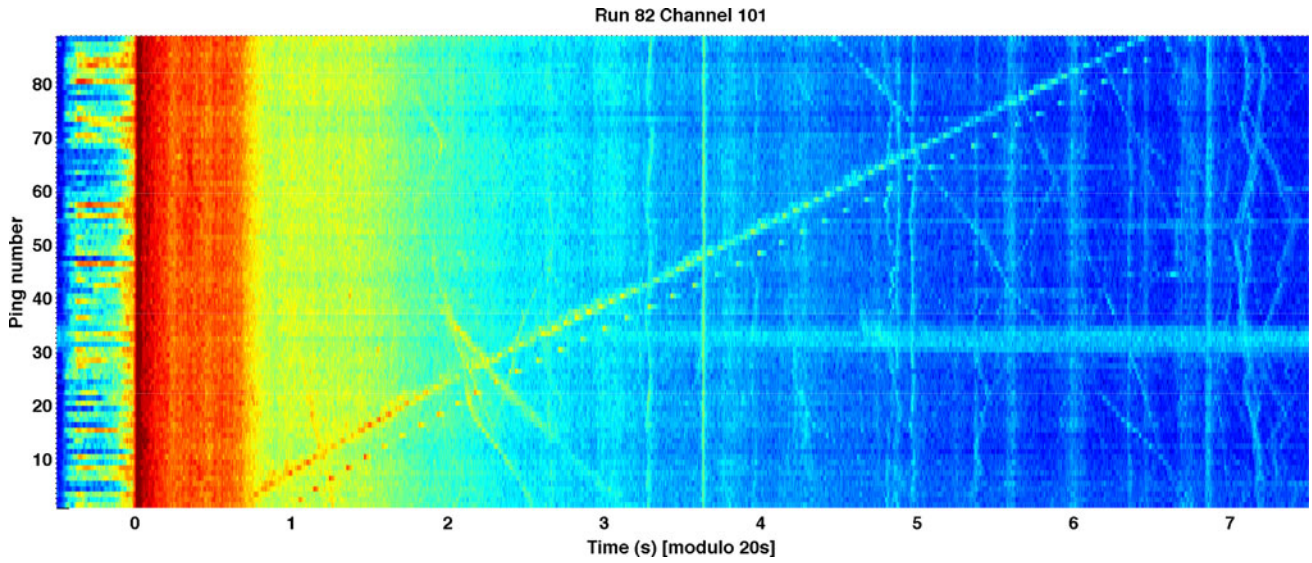

Fig. 5. Run 82, Beam 101 (244° from forward endfire), with *CFAV Quest* steaming outward on the Clutter Track. All 89 pulses are 1800–2700-Hz LFMs, with the initial blast from each pulse lined up to a time of 0 s. *CFAV Quest*'s echo, from lower left to upper right, is seen in each trace; the echo repeater signal, delayed 0.3 s, is seen on alternate pings. Vertical lines represent stationary scatterers.

Short-range model-data comparisons were made with the 10- and 100-ms pulses; Fig. 3 shows model-data differences for two of these pulses out to about 7 s. Bathymetry contours (from the ∼90-m resolution NOAA bathymetry [24]) at 2 m intervals are shown, with the 0- and 2-m contours in white. Many clutter objects are consistent from ping to ping.

There was some indication at the time [9] that near the array (first 2 or 3 s of data) the reverberation was correlated with bathymetry and sand waves, or dunes. Sand dunes and their migration were known in this area [25], so the correspondence with backscatter merited further investigation. With the fine-scale bathymetry data now available, we show there is good correspondence between fluctuations of reverberation intensity and bathymetry (see Section IV-B).

2) TREX13 Data: During TREX13, the same ITC-2015 and FORA system were used. Waveforms as mentioned in Section III-A, both narrowband and broadband, are 0.5 or 1 s long. An example of beamformed results is shown in Fig. 4 using the 1800–2700-Hz LFM signal. The array heading is close to north, ∼356°. In this figure, the uncalibrated data are "normalized" to a prediction from the Clutter Model, with the overall level of the data adjusted to agree near the array. The circle is at 5 s, and the contours are spaced at 5 m.

A number of clutter objects stand out, some corresponding with known wrecks (white diamonds) and deployed equipment (black diamonds). Many of the other clutter objects do not coincide with known bathymetry features or wrecks. The high reverberation just east of the array is likely high scattering and not errors in the bathymetry. The very high reverberation near the shoreline (white contour and black 5-m contour) could be due to due to a number of things: higher scattering, inaccuracies in the model inputs, particularly bathymetry, or even the adiabatic assumption in the model. The agreement of the model and data along the Reverberation Track to the SE is reasonably good; the model inputs, and striations in the reverberation along the Reverberation Track will be discussed in more detail in Section IV.

C. Echo Repeater Data

In TREX13, a number of data sets were taken with *CFAV Quest* towing an echo repeater along the Reverberation and Clutter Tracks. The echo repeater consisted of a source towed immediately behind *CFAV Quest* at a depth of approximately 9 m, and a 16-channel array towed about 70 m behind *CFAV Quest* at depths of 5–10 m to receive the direct transmissions from ITC source. The received signal on one hydrophone was used as a replica for the echo repeater. For the data shown here, the echo repeater was in "ping-pong" mode; that is, each signal was transmitted twice. On the first transmission, the echo repeater recorded and saved the received signal; the second transmission was preceded by a trigger pulse, which then caused the echo repeater to transmit the signal stored from the previous pulse.

Fig. 5 illustrates the received signal on FORA Beam 101 (244° clockwise from forward endfire) during the first half hour of Run 82 (JD130) with *CFAV Quest* towing the echo repeater outward on the Clutter Track. The pulse is the 0.5 s 1.8–2.7 kHz LFM, transmitted every 20 s, so there are 89 pings. On every second pulse, the echo repeater responds, retransmitting the received pulse with a 0-dB gain. To avoid interference with the echo from the hull of *CFAV Quest* a delay of 300 ms was incorporated. The start times of each ping are aligned, so the track of *CFAV Quest* and the echo repeater can be seen on the plot. The echo from *CFAV Quest* can be seen on every ping, and the echo repeater response (delayed 0.3 s) on every second ping. The vertical lines in the plot represent static clutter objects in the beam.[3] One can also see moving scattering objects in the beam, generally moving toward FORA.

Fig. 6 shows the received signal for six pings around the 4-s mark. The echo from *CFAV Quest* can be seen on each ping;

[3]The vertical line at 3.6 s is from the PAT vertical air hose, which is near the ambiguous beam and due to its ∼10–15-dB target strength spills over into this beam.

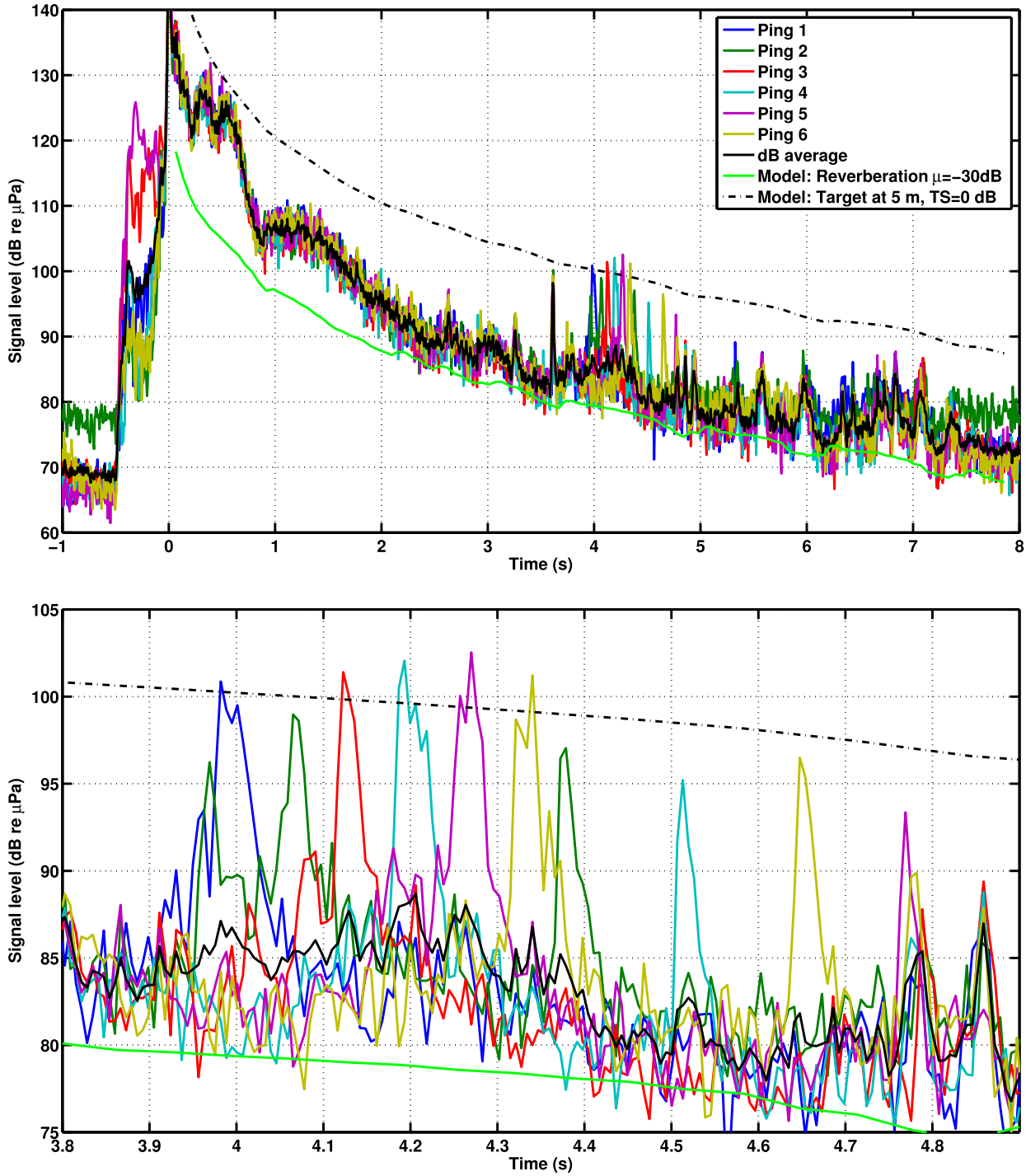

Fig. 6. Signal level for six pings from Run 82, with echo repeater near the "4-s range." The bottom plot is a closeup, illustrating the echo repeater signal delayed 0.3 s on the even pings.

the echo-repeater response, delayed 0.3 s, can be seen on the even pings. For plotting here, the data were smoothed with a Hann window of duration 0.0125 s (39 points) and decimated by a factor of half that (20 points). The echo from *CFAV Quest* is about 5 dB higher than the echo-repeater signal; this suggests a target strength the order of 5 dB for *CFAV Quest* at aft endfire.

IV. Model-Data Comparisons

This section describes the model calculations in more detail. In Section IV-A, the Clutter Model is applied to the TREX site using range-dependent bathymetry and compared with data from the FORA array. Then, the fine scale bathymetry is used with the R2D3 model along a single radial. Along the

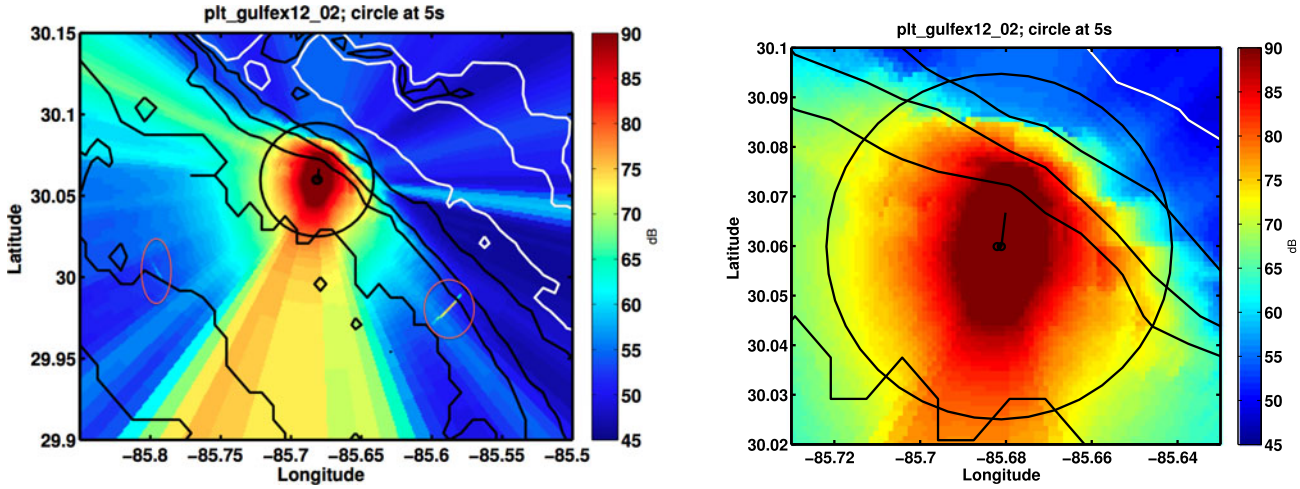

Fig. 7. Left: range-dependent model calculation including beam noise; note how the reverberation is cutoff by the shore contours (0-m contour shown in white). The black circle marks 5 s; the red ovals show target on main and ambiguous beams. Right: short-range enlargement; the effect of depth changes at the grid points (about every 0.01°) can be seen.

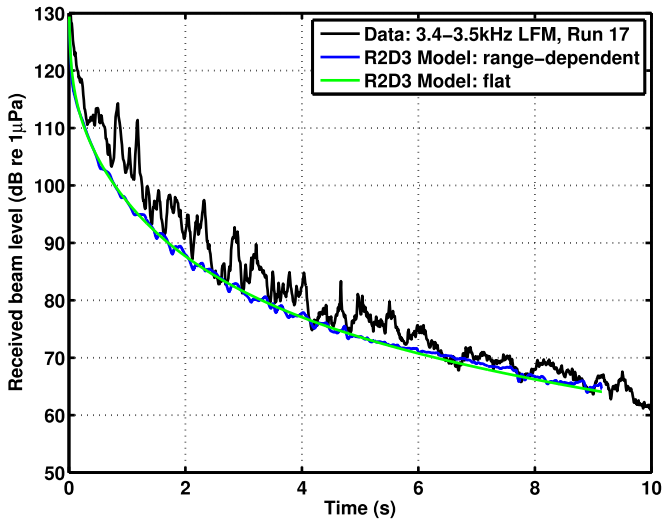

Fig. 8. Model-data comparison for 3400–3500-Hz LFM along main Reverberation Track.

Reverberation Track an interesting correspondence of Reverberation peaks with the bathymetry troughs is observed. The main model-data comparisons are Run 17 (three 200-Hz bands along the Reverberation Track), and Run 82 (1800–2700-Hz LFM, a section of polar plot along the Reverberation Track and a radial along the Clutter Track).

A. Clutter Model Calculations

Fig. 7 shows an illustration of the Clutter Model calculations for a pulse with energy source level ESL = 189 dB re 1 μPa^{2}m^{2}s at 3 kHz; corresponding to the GulfEx 2012 pulse 2500–3500-Hz LFM with SL = 199 dB re 1 μPa^{2}m^2 for 0.1 s. The water was isospeed with sound speed 1530 m/s; the bottom properties [26], from previous experiments in the area, used a half-space with sound speed c_b = 1680 m/s, density $\rho_b = 2040$ kg/m^3, and attenuation $\delta_b = 0.84$-dB/wavelength, or 0.5 dB/(m·kHz). Reverberation was assumed to be due to bottom scattering using Lambert's rule with $\mu = -27$-dB scattering strength. The bathymetry was from General Bathymetric Chart of the Oceans (GEBCO) bathymetry [27] (50 by 56 points on a half-minute grid ∼0.9-km spacing), modified so the minimum water depth was 0.9 m, leaving at least one propagating mode at 3 kHz. The receiver was a horizontal array of 48 elements at 0.2-m spacing, and 157 beams with left–right cardioids were formed. The Clutter Model can accept a different noise level on each beam; for this calculation the measured beam noise from one of the pings was used. There is a 15-dB target at mid depth, 12.7 km to the SE. Calculations were done at a single frequency 3000 Hz, using the average beam patterns over the 2500–3500-Hz band. Using 58 radials reverberation was calculated on all 157 beams every 0.1 s out to 25 s. Calculation time was about 3 min on a 2-GHz laptop.

In the left panel of Fig. 7, one can see how the reverberation is cutoff by the shore contours of the underlying bathymetry. In the short-range enlargement (right panel of Fig. 7), the effect of depth changes at the grid points (about every 0.01°) can be seen. The GEBCO resolution is too coarse for one to see any of the smaller features. Even the NOAA bathymetry ∼90-m resolution is too coarse. In Section IV-B, calculations from the R2D3 model will be shown, using higher resolution bathymetry but along a single radial.

The target echo to the SE appears above the noise, as an arc spreading across several beams (red ellipse). It can be seen faintly to the SW on the ambiguous beam (red ellipse). The effect here is basically a beamwidth effect, since the propagation is dominated by low grazing angle paths. More generally, the 3-D conical beams of a line array can introduce a beam bias. Using the spherical trigonometry relation $\cos\beta = \cos\theta\cos\phi$, e.g., if the scattering (which is small at low grazing angles) is dominated by scattering at steeper grazing angles of say $\theta = 19°$, then scattering from azimuth $\phi = 35°$ from endfire would appear

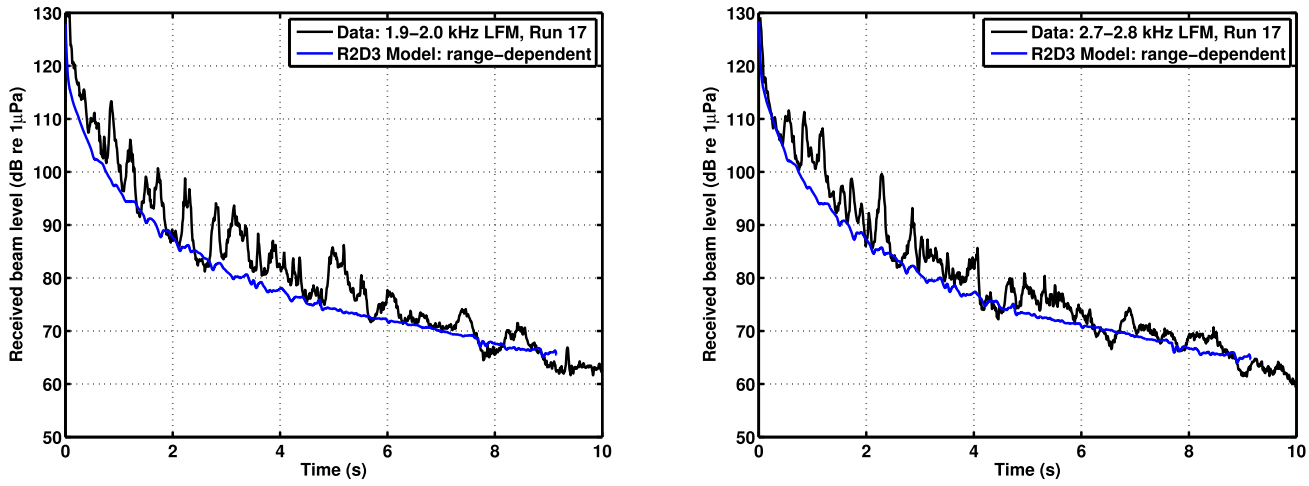

Fig. 9. Model-data comparisons for 1900–2000-Hz and 2600–2700-Hz LFMs from Run 17.

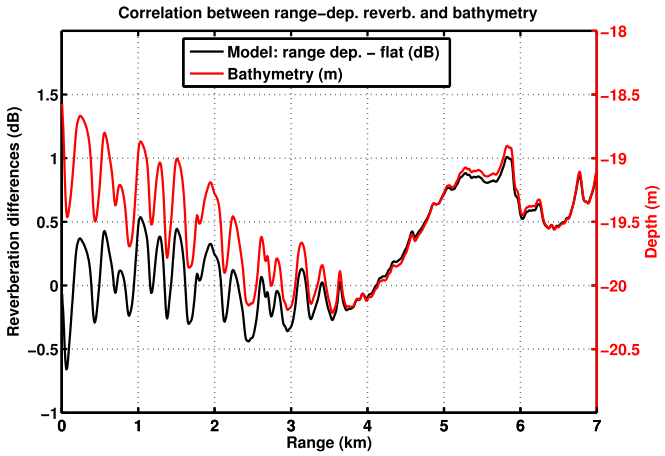

Fig. 10. Difference of flat and range-dependent reverberation predictions along the Reverberation Track, compared with de Moustier's 2013 bathymetry.

on the beam $\beta = 30^\circ$ from endfire. The scattering angles are not likely that high, so the bias will be small, except close to endfire.

B. R2D3 Calculations

To obtain more quantitative results, in this section calculations along a single radial are shown. Fig. 8 shows a comparison of the range-dependent R2D3 model with Run 17 data, from a 10-ping average of the 1 s 3400–3500-Hz LFM at source level 199.8 dB re 1 μPa^{2}m^2. The model was run at 3450 Hz and the omnidirectional results were reduced by the effective reverberation response of 21.3 dB corresponding to $(2\pi)^{-1}$ times the effective beamwidth of the broadside beam of a uniformly weighted array. The same bottom half space as in the previous calculation was used, but the Lambert coefficient was adjusted to -31 dB to get a fit to the bottom envelope of the measured levels. The predicted reverberation is about the correct level, although a slower dropoff at short times and faster dropoff at long times would be better. The flat bottom model prediction follows the trend of the range-dependent prediction quite closely. These model-data comparisons are not meant to be definitive; rather, they are a rapid environmental assessment tool to determine, where we should concentrate for more data analysis and improved environmental inputs.

Similar graphs (see Fig. 9) were obtained for the 1900–2000-Hz LFM and 2700–2800-Hz LFM, with source levels of 196.4 and 197.9 dB re 1 μPa^{2}m^2, and effective reverberation reductions of 18.9 and 20.4 dB, respectively. The data-model differences are similar at the three frequencies, so the source level and beam pattern effects account for most of the frequency dependence in the data. The bottom reflectivity for a half space is frequency independent, and the Lambert coefficient was frequency independent, so it suggests the scattering itself is not strongly frequency dependent.

Note that at short range the data show much higher variations ($\sim$10 dB) than the model prediction ($\sim$1–2 dB). First, we look at the model predictions. Fig. 10 shows the flat-bottom (18-m depth) model prediction subtracted from the range-dependent model prediction using R2D3 with the no-slope option; also shown is the input bathymetric profile. As the water gets shallower, the reverberation increases. This is what we would expect: The mode amplitudes are proportional to $1/\sqrt{H}$, where H is the water depth. Therefore, from (7) for example, the reverberation would be proportional to H^{-2}, giving the calculated 1-dB increase in level when the water depth decreases by 10%. The range-time mapping here and for other TREX13 figures uses a group velocity of 1525 m/s.

The data, however, show the opposite behavior with respect to the bathymetry. Fig. 11 compares the reverberation variations with the black curve representing the difference between the data and a flat bottom model, the red curve the bathymetric fluctuations around the 19-m mean surface, and the green curve the slope of the bathymetry. Note that the depth (red) is positive here, so that the peaks in the reverberation (black) roughly correspond to the dips in the bathymetry—opposite to the model prediction. The bathymetry is from the 10-m version

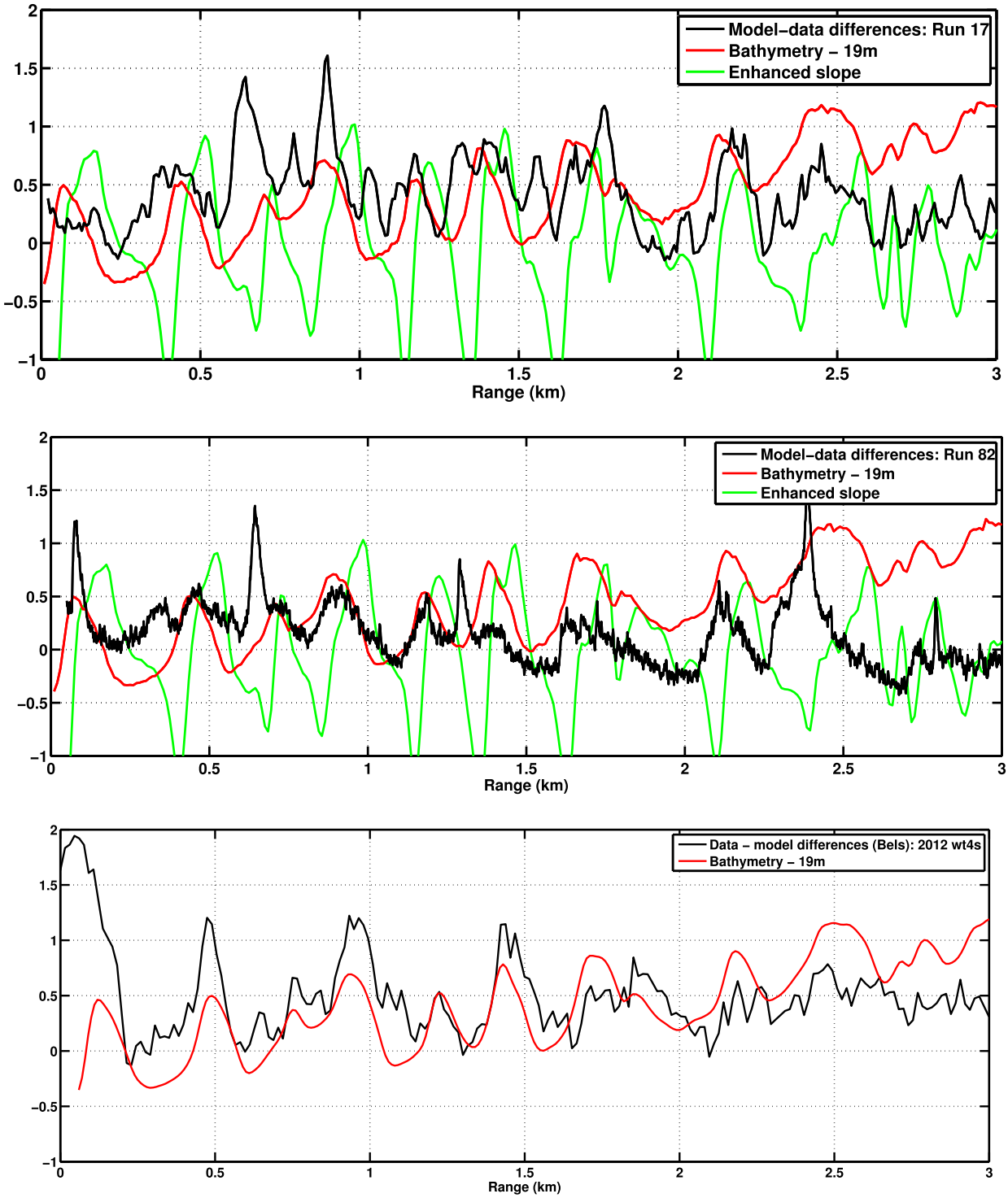

Fig. 11. Correspondence between the averaged reverberation along the Reverberation Track, the bathymetry, and the slope of the bathymetry for Run 17 (upper), Run 82 (middle), and 2012 data (lower). The bathymetric profile is from the acoustic center of the FORA array toward the 7-km point of the Reverberation Track, and offset by 19 m for display. The slope (upward being positive) is increased by a factor of 100. The model-data differences in decibel are reduced by a factor of 10.

of de Moustier's bathymetry, smoothed with a 5-point Hann window. Results from three runs are shown. The upper graph is from Run 17, a 10-ping average of the 3400–3500-Hz LFM processed at APL. The model is as described earlier for Fig. 8. The middle graph shows data from Run 82, the average of the 1800–2700-Hz LFMs processed by the DRDC/Akoostix procedure. The model calculation is at 2250 Hz, with similar environmental inputs, and with the mean reverberation level adjusted to approximate the MF data. The lower graph is from the GulfEx 2012 data, an average of three 2500–3500-Hz LFMs. The model calculation is at 3000 Hz. In this case, the exact position of FORA was not known, and bathymetry has been shifted 50 m along the track to

line up with the reverberation peaks. In each of the three cases, the array orientation is different, so the reverberation track is on a different steering angle of the towed array. The model calculations have taken into account the different effective horizontal beamwidth responses.

Though not the strong correlation with bathymetry and model predictions, there is definitely a good correspondence between the peaks of the measured reverberation and the troughs in the bathymetry. Yang *et al.* [8] have determined correlation coefficients for a number of runs (with some biologic and other transient effects removed). For the first 3 km along the main track a correlation coefficient of 0.75 between the inverted bathymetry and the reverberation levels was obtained. Off the center of the main track the correlation decreases, but is still 0.55 or more over a 40° sector. Fluctuations, and sidelobes will definitely have some effect. The correlation with the slope is not as good. The explanation for the reverberation variations is likely related to the seabed or sub-bottom effects. This points to the need for additional measurements, especially in the trough regions.

The R2D3 model also does target echo calculations. Fig. 6 includes a calculation of reverberation and target echo at 2250 Hz along the Clutter Track. The best estimate of the signal level was 197.6 dB re 1 μPa^{2}m^2 for a duration of 0.5 s, and point target of strength 0 dB was assumed at depth 5 m. The geoacoustic model was the same as for the main reverberation track with a Lambert coefficient of -30 dB. For the reverberation the effective reverberation reduction is 17.3 dB for beam steering angle 245° averaged over the 1800–2700-Hz band. The early reverberation data have some strong undetermined features, but after 2 s the reverberation prediction tracks along the lower envelope of the data. However, to get the model predictions to track the target echo measurements in a reasonable manner, it was necessary to use a slightly downward refracting profile. Since this was a daytime run, a sound-speed profile from an early evening conductivity–temperature–depth (CTD) probe was used. Though only about 3-m/s sound-speed difference between surface and bottom, it makes a considerable difference in the target echo, reducing it the order of 10 dB at 5 km, but having very little effect on the reverberation. More detailed analysis has to be done on comparing with other transmission loss and target echo calculations. For now, it is a demonstration of the diagnostic value of the model calculations toward checking consistency of the reverberation and target echo modeling, and showing the sensitivity of the echo prediction to the sound-speed profile.

V. Discussion

"Knowledge of the fact differs from knowledge of the reason for the fact."—Aristotle

The observed reverberation is a combination of surface, volume, bottom, and sub-bottom scattering. It is assumed the bottom is dominant, with perhaps some sub-bottom penetration in the trenches. For our scattering we have used Lambert's rule, being the simplest and most widely used. A different scattering function will give a somewhat different behavior, but it is a useful way to parametrize the scattering. If the angular dependence of the scattering function is assumed to have a Lambert behavior at all ranges, then a scattering strength can be obtained as a function of range. Fig. 12 shows the implied Lambert scattering strength along the Reverberation Track using some Run 17 data. At any range r, it is the Lambert scattering strength $\mu(r)$ needed to have the model prediction agree with the data. It is simply calculated by taking the difference between the measured data and a corresponding model prediction with a 0-dB Lambert coefficient. The absolute levels, being model-data differences, are only as good as the model predictions and the calibration of the data; e.g., an error of 1 dB in the propagation will produce a 2-dB error in the implied scattering strength. The relative differences at nearby ranges should be reasonably reliable. Analysis of transmission loss measurements will lead to better bottom properties, better estimate of the transmission loss, and better absolute measures of the scattering.

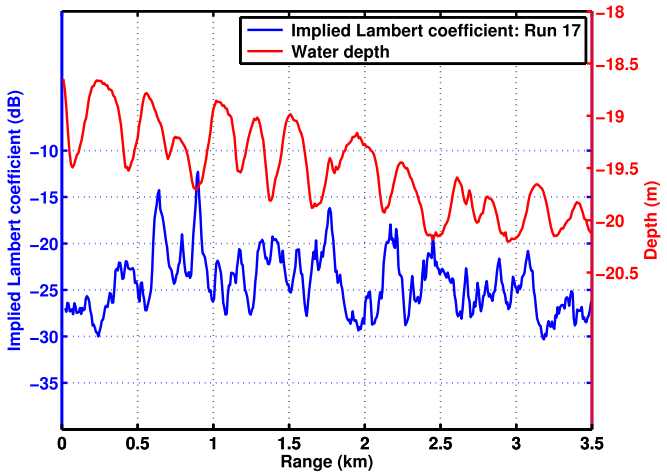

Fig. 12. Implied scattering strength for the TREX13 main reverberation path compared with water depth.

Our values for the geoacoustic parameters were taken from analysis of a previous experiment in the area [26]. Alternate models can give a reasonable fit to the data. For example, in a Pekeris environment with Lambert scattering, the energy flux approximation indicates [28] that the long-range (greater than ~0.5 km here) reverberation is proportional to μ/α^2, where $\alpha \sim \delta_b \rho_b / (c_b^2 \sin^3 \theta_c)$ is the slope of the bottom reflection coefficient at low grazing angles, and θ_c is the critical angle. That means we can get essentially the same model prediction by changing the Lambert coefficient by some factor, and the attenuation coefficient by the square root of the same factor.

Another possibility would be to use a different scattering function, e.g., one based on perturbation theory, which has a $\sin^4$ backscattering behavior at low grazing angles, rather than the Lambert $\sin^2$ behavior, leading to a different range dependence of the reverberation [15]. One could extract a similar implied strength as in Fig. 12, illustrating the same enhanced features in the troughs, but with a different strength and somewhat overall trend.

Fig. 12 also shows the water depth. There is generally enhanced scattering, often the order of 10 dB, from the troughs between the sand waves. For uniform scattering strength, the model predictions (see Fig. 10) predict slightly higher reverberation at the top of the sand dunes, due to the shallower water depth. However, the data clearly show enhanced scattering in the

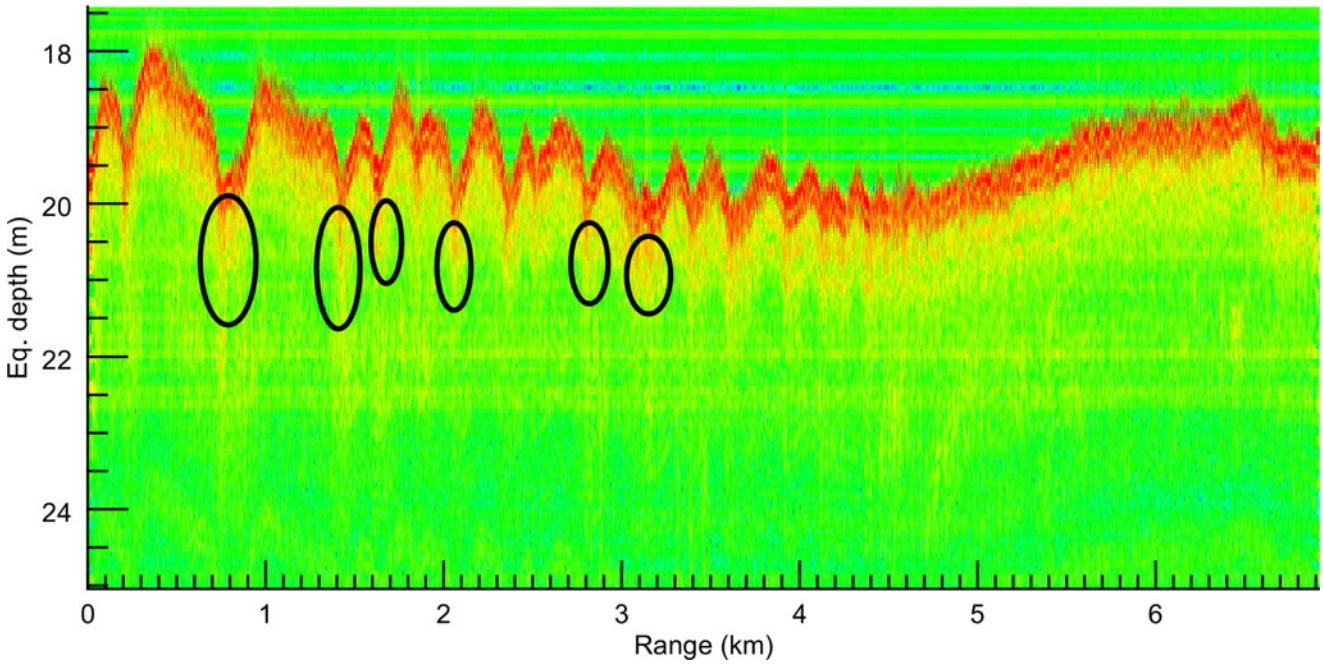

Fig. 13. False color image of return from DRDC sub-bottom profiler along the Reverberation Track showing enhanced penetration in the troughs.

troughs, so the enhanced scattering is not due to the bathymetry itself, but due to some change in the intrinsic scattering due to a different material or mechanism in the troughs. The DRDC sub-bottom profiler towed along the Reverberation Track also shows enhanced penetration in the troughs (see Fig. 13) [29], suggesting a softer material and possibly sub-bottom volume reverberation. Measurements [30] after the sea trial show a softer material in the troughs. There is also some indication that the enhanced scattering may be quite narrow in range [31].

The bathymetry shown is along a single radial; probably several narrowly spaced radials should be used since the beams sample a swath several degrees wide. The single radial model calculation assumes the bathymetry is perpendicular to the radial. If the bathymetry or enhanced scattering ridges are not perpendicular to the radial, then the peaks will be reduced and stretched over time.

The high scattering in the troughs is not confined to the main track. Fig. 14 shows the TREX13 data-model differences of Fig. 4 at short range along the reverberation track. Here, the bottom contours from the 10-m resolution bathymetry are shown. Other than the early portion, the low scattering (blue) seems to be coming from the peaks (white contours) of the dunes, and the high scattering (yellow and red) from the troughs (grey contours).

The model calculations have been quite useful in interpreting the data, and identifying areas of interest where data and model predictions differ. The normal mode formulation can be extended to handle volume reverberation [17] in the water and sub-bottom, or scattering from a sub-bottom interface. However, it is beyond the scope of the paper to pursue these possibilities. The adiabatic mode model is very useful and computationally efficient, but its limitations need to be validated against more elaborate range-dependent models.

VI. Summary

A range-dependent reverberation and target echo model has been developed using adiabatic normal modes for propagation. It can handle towed array beam patterns and bistatic geometry and can make predictions of beam time series that can be compared directly with measured data. This allows many of the effects of the measuring instruments to be removed, with the data-model differences giving useful information about the environment, or where the models need to be enhanced.

The TREX experiments were extremely successful. High quality data were collected, during both daytime and nighttime, for almost a month. The source levels were kept low for environmental reasons, but the directional nature of the FORA array coupled with narrowband LFMs allowed signal to ambient noise out to 5 s and in some cases to 10 s. The area had been chosen to be flat and uniform to facilitate modeling. However, one of the striking features was the relationship of the reverberation features with the sand waves (or dunes) in the area. Although only about 1-m peak-to-trough over several hundred meters range, the dunes resulted in reverberation fluctuations on the order of 10 dB. A key observation is that the peaks in the reverberation usually correspond with the *troughs* of the sand dunes, rather than the crests of the sand dunes. The simple R2D3 model predicts the opposite behavior, and smaller peaks. So this means there are some interesting physics to be explored, which is beyond the scope of this paper. The explanation is likely related to the bottom or sub-bottom effects. Extensive bottom, sub-bottom, and other environmental measurements have been made along this track; these are being investigated by other researchers to facilitate understanding of the reverberation mechanisms, which was indeed the purpose of the TREX13 experiment.

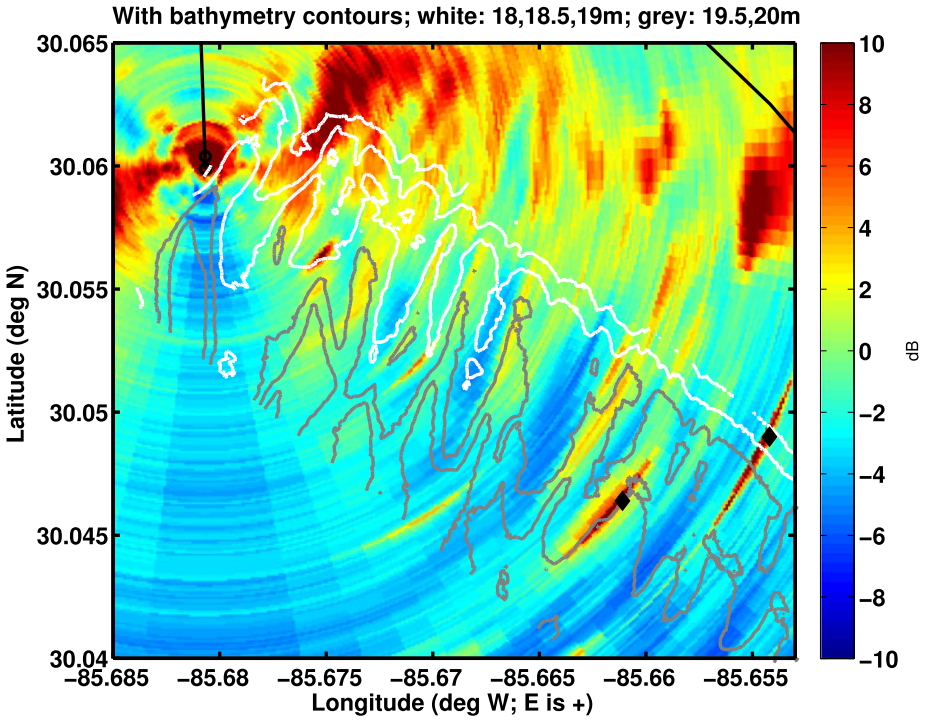

Fig. 14. Polar plot of data-model differences (1800–2700-Hz LFM) at short ranges. Other than the early portion, the low scattering seems to be coming from the peaks (white contours) of the dunes, and the high scattering from the troughs (gray contours). The echoes from the VLA and PAT (black diamonds) are quite noticeable, and spread across several beams.

Some model-data comparisons were made—not to be definitive in any way, but more as a rapid environmental assessment tool to determine where the research team should concentrate for more data analysis and improved environmental measurements. The procedures developed for deep water with poorly known environmental inputs and moving towed arrays [2], [3] were useful in the TREX experiments, where much more detailed environmental information was available. As in earlier experiments, the model-data differences, superimposed on a map of the bathymetry, pointed to areas where more detailed observations were needed. As noted before, the model predictions tell us what we know; the model-data differences point out where we need to investigate further.

Detailed environmental measurements and physics-based models are needed to provide insight into what the scattering mechanisms are. This new understanding can then be incorporated into the model to further improve the performance modeling. The model presented here is computationally efficient, and can handle realistic scenarios, so has potential for active sonar performance modeling.

Appendix A
Calibration of the MF Beamformed Reverberation Levels

To obtain quantitative information about the scattering, it is critical to get the calibrations as accurate as possible. A few issues on calibration, beam forming, and processing are discussed in this section, as they can affect the conclusions (and perhaps the implied physics). The source levels were discussed in Section III-A. Here, we deal with the receiver, beamforming, and matched filtering. In particular, an "exact" calibration for a linear array is presented, and used to validate the MF beam output from a frequency domain processor for the triplet array.

A. Hydrophone Calibration

The FORA triplet array contains 78 elements, each one having three hydrophones (triplets), for a total of 234 channels from the front of the array to the aft end of the array. The data are stored as 4-B integers. The calibration in μPa for the triplet hydrophones is given by

$$L_c = 20\log_{10}(X) + 46.95 - G \tag{14}$$

where L_c is the band level output in decibel re 1 μPa, X is the A/D output integer (24 b), and G is the variable system gain (0, 6, 12, or 18 dB).

B. Triplet Array

In the TREX experiments, the forward module of the triplet array was not working, so the nonacoustic sensors (NAS) and 30 triplets (90 channels) were not available. The aft section was working, including the NAS sensors, so the roll at the end of that section (242°, 242°, 241° for the three deployments) could be obtained, but not the twist. Normally, the roll of each sensor is obtained by interpolating linearly between the forward and aft sensor readings. Mathieu Colin (private communication) looked at individual triplet response for several strong echo repeater signals from Run 75 and suggested a twist on the order of

75°, which would improve the triplet discrimination against the ambiguous beam by about 3 dB.

C. Beamforming and Matched Filtering

The reverberation models are expressed in terms of energy, so we need measured data that are comparable. Three versions of MF output were available for various runs. The ARL/PSU reverberation processing system is briefly described in [2], [34], [35]. It performs a complex band shift filter on the hydrophone data before beamforming with Hann weights and triplet processing [23] based on the NURC procedure [32], [33]. Then, it uses a conventional MF normalization, which for an input pulse of unit amplitude produces a unit response compressed in time, with uncorrelated noise reduced by the time-bandwidth product. The DRDC/Akoostix processing [36] used the ARL/PSU beamformer, but used their own correlator (MF) which was not normalized. The APL processing [8] is done in the frequency domain, using a Gaussian bandpass filter, uniformly weighted elements for beamforming, and an MF normalization that preserves the correct ambient noise level. Here we concentrate on validating that procedure.

To help resolve the issue, a simple procedure was developed. The broadside beam response of a linear array can be obtained with a simple summation

$$B_L(t_n) = \sum_{k=1}^{N_{\rm hp}} w_k s_k(t_n) \tag{15}$$

where $s_k(t)$ are the raw hydrophone time series for the $N_{\rm hp}$ elements of a line array, and the w_k are any weights normalized so that $\sum w_k = 1$. Both uniform $w_k = 1/N_{\rm hp}$ and Hann weights were tested. Equation (15) can be extended to natural beams for which adjacent hydrophones are delayed by an integer number of time samples

$$B_{\rm nb}(t_n) = \sum_{k=1}^{N_{\rm hp}} w_k s_k(t_n + mk/f_s) \tag{16}$$

where f_s is the sampling frequency, and m is an integer 0 (broadside), $\pm 1, \ldots,$. For the TREX 12500-Hz sampling and 0.2-m spacing between elements, only the broadside and $\pm 52.4^\circ$ from endfire were available.

An MF was constructed in the time domain for a pulse of duration T_0

$$M(t_n) = \sum_{j=1}^{N_P} B_L(t_n - \tau_j) r_0(\tau_j) \tag{17}$$

where $r_0(\tau)$ is the normalized pulse replica, with $\sum_{j=1}^{N_P} r_0^2(\tau_j) = 1$; $N_P = f_s T_0$.

This was used to compute various MF outputs. A Tukey pulse $T(F,t)$ with tapering $F/2$ at each end, and with unit rms amplitude has energy

$$I_{\rm Tuk}(F) = \int_0^{T_0} |T(F,t)|^2 \, dt = T_0 \left[1 - \frac{5}{8}F\right]. \tag{18}$$

For $F = 0.2$ and $T_0 = 1$ s, $10 \log_{10} I_{\rm Tuk}(F) = -0.58$ dB.

As a test, the replica was applied to a time series that contained the pulse, as well as a random-phase pulse (i.e., a pulse with the same amplitude spectrum, but with random phases, giving a proxy for reverberation). For a 1-s Tukey-shaded 3.4–3.5-kHz LFM pulse it produced a large spike of unit amplitude and short duration, while for the random-phase pulse it produced a rapidly fluctuating response on the order of 20 dB lower over the duration of the pulse. Note, the full MF response of course extends over $2N_P + 1$ points, or twice the duration of the original pulse. To determine things more precisely, the integrals of the energy in the LFM pulse and random-phase pulse were computed numerically. The integrals of the input LFM and random phase pulse were equal, as were the integrals over the MF output for the pulse spike and the output from the random phase pulse. The ratio of the two were 18.96 dB; i.e., adding 18.96 dB to the conventional MF result gives energy. This corresponds closely with the nominal time-bandwidth product of 20 dB, with the effective time and bandwidth both reduced slightly by the Tukey shading. For a wider bandwidth 2.7–3.6-kHz pulse the effective time-bandwidth product is 28.49 dB.

D. Comparison With Frequency-Domain Processing

Detailed comparisons were made with the APL processing. It uses a frequency-domain MF

$$d(t) = F^{-1}\left\{G(f) \times S(f) \times A(f)^*\right\}. \tag{19}$$

Here, $G(f)$ is the spectrum of a Gaussian noise filter with full 3-dB width equal to the transmitted bandwidth; $S(f)$ is the spectrum of the received signal; $A(f)$ is the conjugate of the spectrum of the drive voltage normalized to its peak value; F is the Fourier transform; and $d(t)$ is the time series after matched filtering. The advantage of this MR is that it preserves the right level of ambient noise when $G(f)$ is renormalized for the loss over the bandwidth (0.7 dB for the beamforming and 1.4 dB for the MF).

Some reverberation data from the broadside beam of the linear array (no triplets) were compared. It is quite satisfying that with $G(f)$ renormalized the frequency-domain processing of (19) and the time-domain beamforming and MF of (15) and (17) agree almost identically.

Due to the low sampling rate and closely spaced hydrophones in the triplets there was no simple way analogous to (15) to test the triplet beamforming [33]. However, the linear array beamformed results (15)–(17) can be used to validate the triplet beamformed results. First, the linear array has the left–right ambiguity so when one beam of the triplet array has a feature much stronger than its ambiguous beam, the stronger beam should agree quite closely with the corresponding beam of the linear array. Second, because of the left–right cardioids, the linear beamformed results are close to the addition of left and right beamformed results from a triplet. There is a small error since each cardioid will reduce the nonhorizontal arrivals from the side it is steered, but will pick up some energy from its response on the back side.

Fig. 15 shows the comparison between linear and triplet beamformed results at broadside and the natural beam at 52°

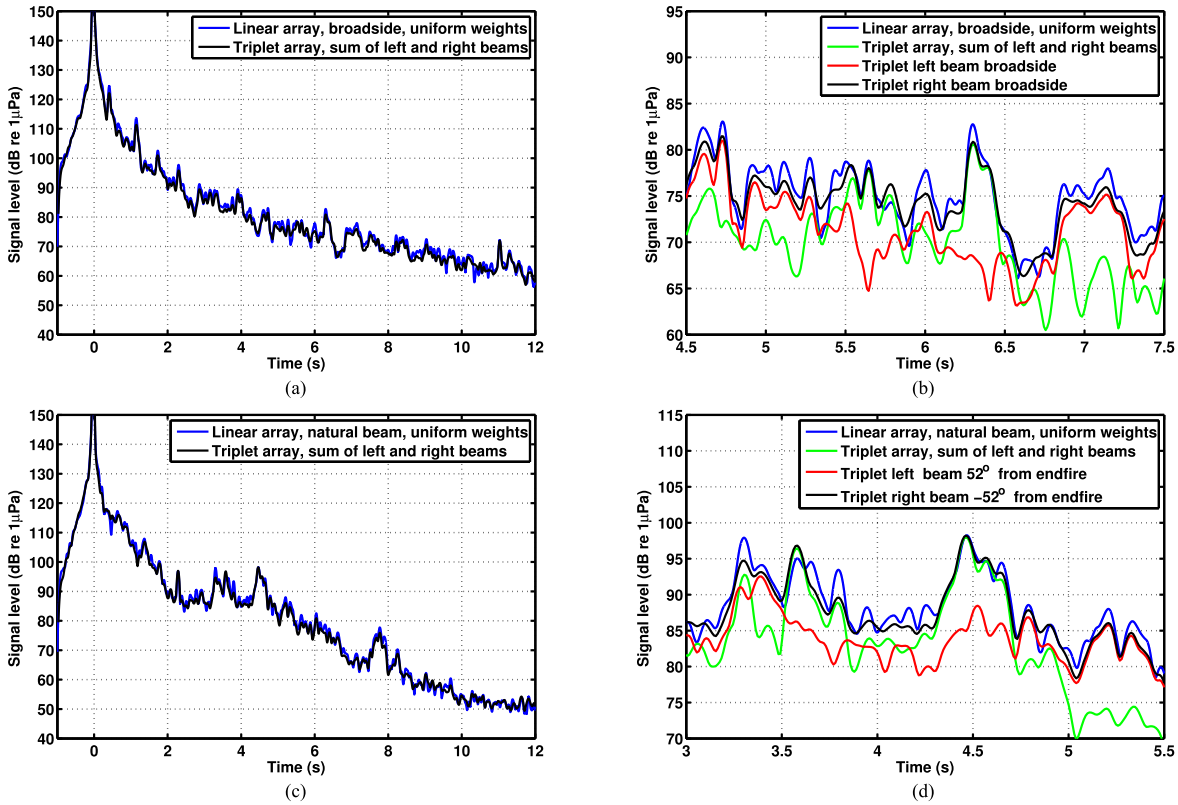

Fig. 15. Comparisons between triplet and linear array beamformed results. Broadside: (a) linear versus summation of left and right broadside beams of a triplet case and (b) zoom-in of (a) with two additional curves representing the individual left and right broadside beams of a triplet. Natural beam (52° referenced to endfire): (c) linear versus summation of ±52° beams of a triplet case and (d) zoom-in of (c) with two additional curves representing the individual ±52° beams of a triplet.

referenced to endfire. Fig. 15(a) and (b) shows the broadside cases. The linear array beamformed results are almost identical to the summation of the left and the right beams from the triplet processing. The zoomed-in plot in Fig. 15(b) displays the individual left and right beams of the triplet, which demonstrates nicely that the features are different but the summation of the two beams is very close to the linear results. All results here included 1.4 dB to obtain absolute level. Fig. 15(c) and (d) shows similar results but along the 52° natural beam. Excellent agreement is achieved similar to the broadside case.

E. Procedure Applied to Uncalibrated Data

In addition to confirming the frequency-domain processing, the simple procedure can be used to obtain an approximate energy calibration of uncalibrated MF output. Fig. 16 shows a similar result applied to uncalibrated beam output, with Hann weights for the beamforming. The left and right broadside beams and their energy sum have been offset by the same amount, to provide reasonable overall agreement with the levels of the simple linear array procedure. A close up of a section is shown, and the offset provides the calibration factor needed for the uncalibrated beam output. Comparisons (not illustrated) were made, showing good agreement for some natural beams and for different pulse types.

In summary, an approximate calibration procedure can be applied to uncalibrated data.

1) Ensure the output from each hydrophone is uniformly calibrated.

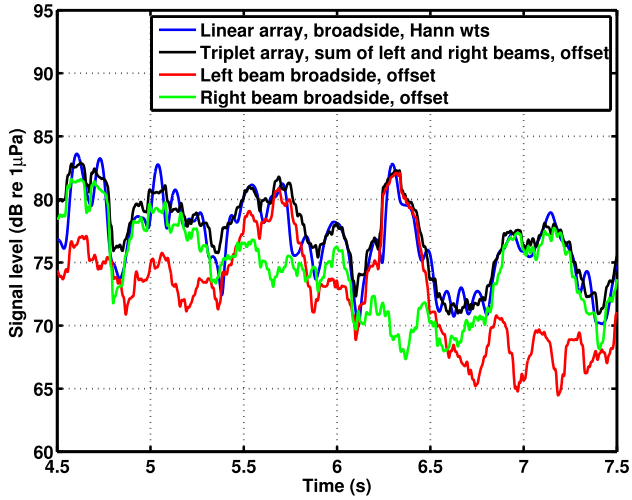

Fig. 16. Comparison of the simple procedure applied to unprocessed MF beam output.

2) Apply the Gaussian bandpass filter to the hydrophone time series.
3) Calculate the broadside beam, including the calibration factor for μPa and correcting for the Gaussian filter loss.
4) Apply the MF to the beam, adding the effective time-bandwidth product for the pulse to the conventional normalization.
5) Compare the left and right processed beams with the simple procedure, (15) and (17).

6) Use the difference between the simple procedure and the processed MF time series as an approximate calibration.

This would seem to be almost as accurate as the knowledge of the source levels and array calibrations over the band of interest.

With the data calibrations in hand, the source energy level for modeling should be reduced by 0.6 dB from the nominal source level $\times$ pulse length approximation, due to the 10% Tukey shading of the pulse. For a monostatic reverberation model with omnidirectional beam patterns (e.g., R2D3), the reduction in level by a particular of the towed array beam can be approximated with the effective reverberation response, which acts as a horizontal beamwidth [15].

ACKNOWLEDGMENT

T. Hefner, D. J Tang, and K. Williams from APL/UW planned and directed the experiments. P. Hines from DRDC Atlantic was the Chief Scientist on the DRDC research vessel *CFAV Quest*. Akoostix Inc., Dartmouth, NS, Canada, processed data for DRDC. M. Colin from TNO (The Netherlands) spent a week aboard *CFAV Quest* during TREX13, and was very helpful in getting a quick look at the data. Support from the crew and staff on *CFAV Quest* and *R/V Sharp* are most appreciated. D. J. Tang, T. Hefner, and other co-workers from APL/UW provided useful inputs and discussions. The multibeam bathymetry was provided by C. de Moustier and co-workers. The authors would like to thank the anonymous reviewers for their valuable comments.

REFERENCES

[1] J. R. Preston, T. Akal, and J. Berkson, "Analysis of backscattering data in the Tyrrhenian Sea," *J. Acoust. Soc. Amer.*, vol. 87, pp. 119–134, 1991.

[2] J. R. Preston and D. D. Ellis, "Extracting bottom information from towed-array reverberation data—Part I: Measurement methodology," *J. Mar. Syst.*, vol. 78, pp. S359–S371, 2009.

[3] D. D. Ellis and J. R. Preston, "Extracting bottom information from towed-array reverberation data—Part II: Extraction procedure and modelling methodology," *J. Mar. Syst.*, vol. 78, pp. S372–S381, 2009.

[4] K. M. Becker and J. R. Preston, "The ONR Five Octave Research Array (FORA) at Penn State," in *Proc. IEEE OCEANS Conf.*, Sep. 2003, pp. 2607–2610.

[5] D. Tang and B. T. Hefner, "Measurement issues in mid-frequency reverberation experiments," in *Proc. 11th Eur. Conf. Underwater Acoust.*, 2012, pp. 1499–1504.

[6] B. T. Hefner and D. Tang, "Overview of the reverberation component of TREX13," in *Proc. 2nd Underwater Acoust. Conf. Exhib.*, 2014, pp. 707–713.

[7] J. R. Preston, "Some results from the very shallow water TREX13 reverberation experiments using the Five Octave Research Array triplet module," *Proc. Meetings Acoust.*, vol. 20, 2013, Art. no. 070003.

[8] J. Yang, D. Tang, B. T. Hefner, K. L. Williams, and J. R. Preston, "Overview of mid-frequency reverberation data acquired during the 2013 Target and Reverberation Experiment, " *IEEE J. Ocean. Eng.*, to be published.

[9] D. D. Ellis and J. R. Preston, "Comparison of model predictions with reverberation and clutter data in a range-dependent shallow water area," in *Proc. 1st Underwater Acoust. Conf. Exhib.*, 2013, pp. 465–472.

[10] D. D. Ellis, J. Yang, S. Pecknold, and J. R. Preston, "Correlation of reverberation with bottom sand waves along the TREX reverberation track," in *Proc. 2nd Underwater Acoust. Conf. Exhib.*, 2014, pp. 715–722.

[11] H. P. Bucker and H. E. Morris, "Normal-mode reverberation in channels or ducts," *J. Acoust. Soc. Amer.*, vol. 44, pp. 827–828, 1968.

[12] D. D. Ellis, "A shallow-water normal-mode reverberation model," *J. Acoust. Soc. Amer.*, vol. 97, pp. 2804–2814, 1995.

[13] D. D. Ellis, "Normal-mode models OGOPOGO and NOGRP applied to the 2006 ONR Reverberation Modeling Workshop problems," DRDC Atlantic, Dartmouth, NS, Canada, Tech. Memo. TM 2006–289, Jun. 2008.

[14] D. D. Ellis, "Effective vertical beam patterns for ocean acoustic reverberation calculations," *IEEE J. Ocean. Eng.*, vol. 16, no. 2, pp. 208–211, Apr. 1991.

[15] M. A. Ainslie and D. D. Ellis, "Echo, reverberation, and echo-to-reverberation ratio for a short pulse in a range-dependent Pekeris waveguide," *IEEE J. Ocean. Eng.*, vol. 42, no. 2, Apr. 2017, DOI: 10.1109/JOE.20172658738.

[16] D. D. Ellis, J. R. Preston, P. C. Hines, and V. W. Young, "Bistatic signal excess calculations over variable bottom topography using adiabatic normal modes," in *Proc. Int. Symp. Underw. Reverberation Clutter*, NATO Undersea Research Centre, La Spezia, Italy, 2008, pp. 97–104.

[17] D. D. Ellis, T. J. Deveau, and J. A. Theriault, "Volume reverberation and target echo calculations using normal modes," in *Proc. MTS/IEEE OCEANS Conf.*, vol. 1. Piscataway, NY, USA: IEEE, Oct. 1997, pp. 608–611.

[18] D. D. Ellis and J. R. Preston, "DRDC Clutter Model: Range-dependent predictions compared with towed array reverberation and clutter data from the Malta Plateau," in *Proc. 4th Int. Conf. Exhib. Underwater Acoust. Meas.: Technol. Results*, 2011, pp. 657–664.

[19] D. D. Ellis, J. R. Preston, and G. H. Brooke, "Progress on the DRDC Clutter Model," in *Proc. 11th Eur. Conf. Underwater Acoust.*, 2012, pp. 1542–1549.

[20] D. D. Ellis, "A two-ended shooting technique for calculating normal modes in underwater sound propagation," Defence Research Establishment Atlantic, Dartmouth, NS, Canada, DREA Rep. 85/105, Sep. 1985.

[21] M. A. Ainslie, D. D. Ellis, and C. H. Harrison, "Low frequency bottom reverberation in a Pekeris waveguide with Lambert's rule," *J. Comput. Acoust.*, vol. 24, no. 2, 2016, Art. no. 1650001. DOI:10.1142/S0218396X16500016.

[22] S. Murphy, P. Hines, and K. Dunphy, "Classifying continuous active sonar echoes for target recognition," in *Proc. 2nd Underwater Acoust. Conf. Exhib.*, 2014, pp. 811–818.

[23] J. R. Preston, "Using triplet arrays for reverberation analysis and inversions," *IEEE J. Ocean. Eng.*, vol. 32, no. 4, pp. 879–896, 2007.

[24] National Ocean Service Hydrographic Data Base, Boulder, CO, USA, 2013.

[25] B. J. Kraft and C. de Moustier, "Detailed bathymetric surveys offshore Santa Rosa Island, FL: Before and after Hurricane Ivan (September 16, 2004)," *IEEE J. Ocean. Eng.*, vol. 35, no. 3, pp. 453–470, 2010.

[26] P. C. Hines, J. C. Osler, J. G. E. Scrutton, and L. J. S. Halloran, "Time-of-flight measurements of acoustic wave speed in a sandy sediment at 0.6–20 kHz," *IEEE J. Ocean. Eng.*, vol. 35, no. 3, pp. 502–515, 2010.

[27] "General Bathymetric Chart of the Oceans (GEBCO): The GEBCO_08 Grid," Intergovernmental Oceanographic Commission (IOC) (of UNESCO) and the International Hydrographic Organization (IHO), British Oceanographic Data Centre, UK, Tech. Rep., 2010. [Online]. Available: http://www.gebco.net/data_and_products/gridded_bathymetry_data/documents/gebco_08.pdf (data file is gebco_08.nc, version 20100927)

[28] C. Harrison and P. Nielsen, "Separability of scattering and reflection parameters in reverberation inversion," NATO Undersea Research Centre, La Spezia, Italy, NURC Report NURC-PR-2007–019, Nov. 2007.

[29] S. Steele and S. Pecknold, "Modelling of seafloor reverberation in northern Gulf of Mexico sandy sediment," *Can. Acoust.*, vol. 43, no. 3, pp. 164–165, 2015.

[30] B. T. Hefner and D. Tang, "Environmental measurements collected during TREX13 to support acoustic modeling," *J. Acoust. Soc. Amer.*, vol. 136, p. 2267, 2014 (abstract only).

[31] C. de Moustier and B. J. Kraft, "Persistence of sharp acoustic backscatter transitions observed in repeat 400 kHz multibeam echosounder surveys offshore Panama City, Florida, over 1 and 24 months," *J. Acoust. Soc. Amer.*, vol. 136, p. 2267, 2014 (abstract only).

[32] D. T. Hughes, "Aspects of cardioid processing," SACLANT Undersea Research Centre, La Spezia, Italy, SACLANTCEN Rep. SR-329A, May 2000.

[33] G. Haralabus and A. Baldacci, "Unambiguous triplet array beamforming and calibration algorithms to facilitate an environmentally adaptive active sonar concept," in *Proc. OCEANS Conf. Boston, MA, USA*, 15–21 Sep. 2006, DOI: 10.1109/OCEANS.2006.307115.

[34] J. R. Preston and D. D. Ellis, "Extracting bottom information from towed-array reverberation data: Measurement methodology," DRDC Atlantic, Dartmouth, NS, Canada, Tech. Rep. TR 2009–042, Sep. 2009.

[35] J. R. Preston, "Shallow water ocean reverberation data analysis and extraction of seafloor geo-acoustic parameters below 4 kHz," Ph.D. dissertation, Acoust. Dept., The Pennsylvania State Univ., State College, PA, USA, Aug. 2002.
[36] J. D. Hood and B. Glessing, "SPPACS maintenance and enhancement," DRDC Atlantic, Dartmouth, NS, Canada, DRDC Contractor Rep. 2005–252, Apr. 2007.

Dale D. Ellis (M'91) received the B.Sc. degree in mathematics and physics from Mount Allison University in Sackville, NB, Canada, in 1970, and the M.Sc. and Ph.D. degrees in theoretical nuclear physics from McMaster University, Hamilton, ON, Canada, in 1971 and 1976, respectively.

He was with the Defence Research and Development Canada, Atlantic Research Center (formerly DREA), Dartmouth, NS, Canada, for 37 years, except for a four-year posting at the NATO Underwater Research Center (now CMRE) in Italy. He is currently an Adjunct Professor at Mount Allison University, Sackville, NB, Canada, and also at Dalhousie University, Halifax, NS, Canada. He helped with the design of the experiments, participated in the gathering, processing, and validation of the data and environmental inputs, developed the reverberation and target echo models, performed the model-data comparisons and estimation of scattering strengths, developed the procedure for validating the matched filter calibrations, and prepared the manuscript. He has participated in approximately 20 sea trials, many of them international collaborations. His current research interests include numerical modeling of shallow-water propagation, reverberation and target echo, and using the predictions to interpret data gathered at sea.

Dr. Ellis is a Fellow of the Acoustical Society of America.

Jie Yang received the B.S. degree in physics from the Ocean University of Qingdao, Qingdao, China, in 1999 and the Ph.D. degree in mechanical engineering from the Georgia Institute of Technology, Atlanta, GA, USA, in 2007.

Since 2007, she was a Postdoctoral Fellow supported by the U.S. Office of Naval Research and then a Physicist with the Applied Physics Laboratory, University of Washington, Seattle, WA, USA. She processed much of the reverberation data, provided accurate source, and FORA positions for correlation with the bathymetry, supplied additional model inputs, worked on the calibrations, and had considerable input to the written manuscript, especially the Appendix on the calibrations. Her research interests include both active and passive acoustics, with the former focusing on mid-frequency sound propagation and reverberation in littoral oceans, and the latter on estimating wind speed and rainrate using ocean ambient sound and their relation to global water cycle and climate change.

Dr. Yang is a member of the Acoustical Society of America.

John R. Preston (M'76–LM'12) received the B.S. degree in physics from the University of Massachusetts, Amherst, MA, USA, in 1967, the M.S. degree in physics from the University of Maryland, College Park, MD, USA, in 1973, the M.S.E.E. degree in electrical engineering from George Washington University, Washington, DC, USA, in 1981, and the Ph.D. degree in acoustics from The Pennsylvania State University, State College, PA, USA, in 2002.

He is an emeritus researcher with the Applied Research Laboratory, The Pennsylvania State University, having worked there from 1995 to 2015 as a Senior Research Associate. His work focused on the Acoustics Clutter Program at the U.S. Office of Naval Research (ONR), Arlington, VA, USA, on the inversion algorithms with the U.S. Naval Air Warfare Center and the ONR, and with NATO Undersea Research Center (NURC) on rapid environmental assessment technology. These efforts are focused on understanding sea bottom reverberation and clutter. He also worked on broadband underwater propagation issues. From 1989 to 1994, he worked at the NURC, La Spezia, Italy, where he planned, executed, analyzed, and led various reverberation experiments using acoustic arrays. Prior to this, he was a Vice-President at Amron Corporation, Washington, DC, USA, where he worked on problems associated with underwater propagation and signal processing. His main contributions were collecting the 2012 and 2013 FORA reverberation data, ensuring its quality, and providing beam time series of data before and after beamforming.

Dr. Preston is a Fellow of the Acoustical Society of America.

Sean Pecknold received the Ph.D. degree in physics from McGill University, Montreal, QC, Canada, in 2000.

He is currently a Defence Scientist in the Underwater Sensing Section, Defence Research and Development Canada's Atlantic Research Center, Dartmouth, NS, Canada, where he is working on acoustic propagation modeling and geoacoustic parameter estimation.

Dr. Pecknold's main contributions to this paper were processing the DRDC reverberation and target echo data, and analysis of the sub-bottom profiler data and preparation of Fig. 13.

DOCUMENT CONTROL DATA

*Security markings for the title, authors, abstract and keywords must be entered when the document is sensitive

1. ORIGINATOR (Name and address of the organization preparing the document. A DRDC Centre sponsoring a contractor's report, or tasking agency, is entered in Section 8.)

DRDC – Atlantic Research Centre
Defence Research and Development Canada
9 Grove Street
P.O. Box 1012
Dartmouth, Nova Scotia B2Y 3Z7
Canada

2a. SECURITY MARKING (Overall security marking of the document including special supplemental markings if applicable.)

CAN UNCLASSIFIED

2b. CONTROLLED GOODS

NON-CONTROLLED GOODS
DMC A

3. TITLE (The document title and sub-title as indicated on the title page.)

A normal mode reverberation and target echo model to interpret towed array data in the Target and Reverberation Experiments

4. AUTHORS (last name, followed by initials – ranks, titles, etc., not to be used)

Ellis, D.D.; Yang, J.; Preston, J.; Pecknold, S.

5. DATE OF PUBLICATION (Month and year of publication of document.)	6a. NO. OF PAGES (Total pages, including Annexes, excluding DCD, covering and verso pages.)	6b. NO. OF REFS (Total references cited.)
February 2018	18	36

7. DOCUMENT CATEGORY (e.g., Scientific Report, Contract Report, Scientific Letter.)

External Literature (P)

8. SPONSORING CENTRE (The name and address of the department project office or laboratory sponsoring the research and development.)

DRDC – Atlantic Research Centre
Defence Research and Development Canada
9 Grove Street
P.O. Box 1012
Dartmouth, Nova Scotia B2Y 3Z7
Canada

9a. PROJECT OR GRANT NO. (If appropriate, the applicable research and development project or grant number under which the document was written. Please specify whether project or grant.)	9b. CONTRACT NO. (If appropriate, the applicable number under which the document was written.)

10a. DRDC PUBLICATION NUMBER (The official document number by which the document is identified by the originating activity. This number must be unique to this document.)	10b. OTHER DOCUMENT NO(s). (Any other numbers which may be assigned this document either by the originator or by the sponsor.)
DRDC-RDDC-2018-P019	

11a. FUTURE DISTRIBUTION WITHIN CANADA (Approval for further dissemination of the document. Security classification must also be considered.)

Public release

11b. FUTURE DISTRIBUTION OUTSIDE CANADA (Approval for further dissemination of the document. Security classification must also be considered.)

12. KEYWORDS, DESCRIPTORS or IDENTIFIERS (Use semi-colon as a delimiter.)
13. ABSTRACT/RESUME (When available in the document, the French version of the abstract must be included here.)